Higgs boson observation and measurements of its properties in the HZZ4 decay mode

Nikolopoulos, Konstantinos; Korytov, A

DOI:
10.1142/9789814425452_0005

Document Version
Peer reviewed version

Citation for published version (Harvard):
Nikolopoulos, K & Korytov, A 2016, Higgs boson observation and measurements of its properties in the HZZ4 decay mode. in A Nisati & V Sharma (eds), *Discovery of the Higgs Boson.* World Scientific, pp. 127-178. https://doi.org/10.1142/9789814425452_0005

Chapter 5

Higgs boson observation and measurements of its properties in the $H \to ZZ \to 4\ell$ decay mode

Andrey Korytov[1] and Konstantinos Nikolopoulos[2]
[1] *University of Florida, Gainesville, FL 32611 USA*
[2] *University of Birmingham, Birmingham, B15 2TT, UK*

In their searches for the Standard Model (SM) Higgs boson in the mass range 115-1000 GeV, both ATLAS and CMS Collaborations observed a narrow four-lepton resonance with a mass near 125 GeV with local significances in excess of 5σ. In the combination of the ATLAS and CMS $H \to ZZ \to 4\ell$ measurements, the mass of the observed boson was found to be 125.15 ± 0.37 (stat) ± 0.15 (syst) GeV. The event rates attributed to the signal and the studied differential cross sections were compatible with the SM Higgs boson hypothesis. Kinematic properties of leptons in signal candidate events agreed with those expected for a state with spin-parity quantum numbers of the SM Higgs boson ($J^P = 0^+$) and strongly disfavoured states with alternative quantum numbers or 0^+ states with non SM-like tensor structures of their couplings to Z bosons. The yield and kinematic properties of events in the high four-lepton mass region allowed one to probe off-shell production of the discovered boson and set model-dependent upper limits on its total width.

1. Introduction

The $H \to ZZ \to 4\ell$ channel*, where ℓ denotes electrons and muons, provides excellent sensitivity to the SM Higgs boson in a broad mass range and is often referred to as the "golden channel". The $H \to ZZ \to 4\ell$ channel was one of the key benchmarks that defined the designs of the ATLAS and CMS experiments. The main virtues of this channel are the fully reconstructed final state of four leptons; the excellent, experimentally attainable four-lepton mass resolution; and the outstanding signal-to-background ratio. Despite the small expected branching fraction, this channel was the

*In this chapter, intermediate on-shell and off-shell Z bosons as well as γ^*, when allowed, are commonly referred to as Z, unless explicitly stated otherwise.

most sensitive for discovering a SM Higgs boson in the mass ranges 120−150 and above 180 GeV [1,2]†.

The number of $H \to ZZ \to 4\ell$ events expected to be produced in the LHC Run 1 ranged from a few to about two hundred, depending on the assumed Higgs boson mass, m_H. The branching fraction, $\mathcal{B}(H \to 4\ell)$, for a SM Higgs boson with $m_H = 125$ GeV is 1.25×10^{-4} [3], implying fewer than 70 four-lepton events per experiment. This is the lowest signal event yield among all decay channels presented in this book. After accounting for detector acceptance, lepton reconstruction and event selection efficiencies, the expected number of detectable signal events was reduced to about 20.

Thanks to the narrow intrinsic width of the SM Higgs boson in the low mass range and the excellent electron and muon momentum reconstruction of the ATLAS and CMS experiments, such a signal would manifest itself as a narrow peak in the four-lepton mass distribution. For a SM Higgs boson with a mass below 300 GeV, the instrumental four-lepton mass resolution of about 1-2% was expected to dominate over the Higgs boson natural width.

The final state with four prompt leptons also ensured small background since such a signature was not characteristic of QCD processes. The main background in this search was electroweak non-resonant di-boson production ($q\bar{q} \to ZZ \to 4\ell$) with a relatively small and well-understood cross section. The narrow signal peak over the continuous distribution of the low-rate background gave rise to a good signal-to-background ratio, 2:1 or higher, for the entire mass range considered in the search. The signal-to-background ratio for the $H \to ZZ \to 4\ell$ channel is the best among all SM Higgs boson decay modes. Moreover, angular and dilepton mass distributions of four well-reconstructed leptons provided rich information on physics underlying four-lepton production processes, which allowed ATLAS and CMS to enhance the signal-vs-background separation even further.

Finally, this channel provided excellent means for studying the properties of the discovered boson. The narrow mass peak and high signal-to-background ratio facilitated precise mass measurements and studies of production-related properties, such as the Higgs boson's transverse momentum, multiplicities of jets produced in association with the Higgs boson, etc.. The kinematics of the four final state leptons, being sensitive to helicity amplitudes of Z bosons produced in $X \to ZZ$ decays, allowed for detailed studies of the spin-parity properties of the discovered boson. The relative production rates of off-shell $H^* \to ZZ \to 4\ell$ and on-peak

†In the mass ranges below 120 and $150 - 200$ GeV, the branching fraction for the SM Higgs boson is impractically small, as discussed in Chapter **??**.

$H \to ZZ \to 4\ell$ events was used for probing, albeit with some model-dependent assumptions, the natural width of the observed boson.

Unless stated otherwise, the experimental results presented in this chapter are based on Refs. [4–13].

2. Physics objects used in the analysis

The physics objects used in the $H \to ZZ \to 4\ell$ analyses are leptons, photons, and jets. The reconstruction specifics relevant to this channel are discussed below, while the general description of physics object reconstruction can be found in Chapter **??**.

2.1. *Electrons and muons*

With at least four leptons in the final state, the search for a Higgs boson in the $H \to 4\ell$ decay mode and measurements of the discovered boson's properties demanded a high pseudorapidity acceptance and a high reconstruction efficiency for leptons.

Figure 5.1 (a) shows the pseudorapidity, η, distribution for the highest-pseudorapidity lepton originating from decays of Higgs boson with $m_H = 125$ GeV, produced via gluon fusion at $\sqrt{s} = 8$ TeV. The probability that all four leptons would have pseudorapidity $|\eta| < 2.4$ (muon detector acceptance in CMS) is only 66%. Acceptance for muons in ATLAS was $|\eta| < 2.7$. Electrons in ATLAS and CMS were reconstructed within $|\eta| < 2.5$.

Efficient reconstruction of low-p_{T} leptons (p_{T} <10 GeV) was of a particular importance. In the low Higgs boson mass range ($m_H < 2\,m_Z$), at least one Z boson originating from the $H \to ZZ$ decay is off-shell and gives rise to relatively low-p_{T} leptons. For $m_H = 125$ GeV, the typical invariant mass of such off-shell Z bosons is only about 35 GeV. Figure 5.1 (b) shows the p_{T} distribution of leptons for $m_H = 125$ GeV, ordered by their p_{T}, for events with all four leptons within the detector acceptance. Less than 80% (40%) of these events would have all leptons with $p_{\mathrm{T}} > 5$ (10) GeV.

Thus, both ATLAS and CMS made sure that their detector designs and lepton reconstruction algorithms allowed for reconstructing muons and electrons with transverse momenta as low as 5-7 GeV. No other Higgs boson analysis described in this book had to face the experimental challenges associated with using so low-p_{T} leptons. The "turn-on" of the muon reconstruction efficiency, shown on example of ATLAS in Fig. 5.2 (a), was near $p_{\mathrm{T}} \sim 3$ GeV. The efficiency "turn-on" for electrons was at $p_{\mathrm{T}} \sim 7$ GeV.

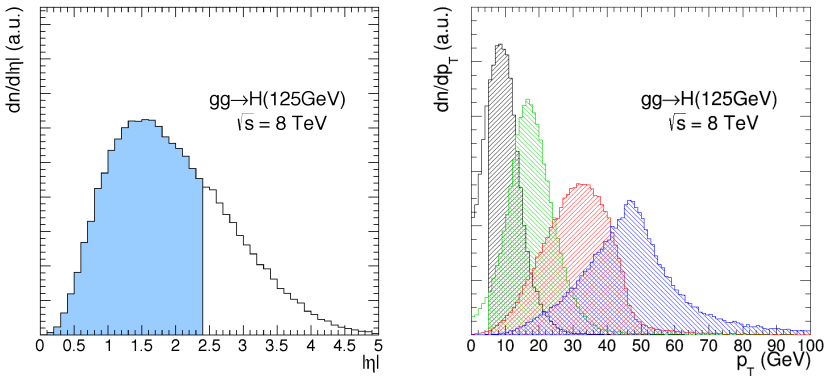

(a) (b)

Fig. 5.1. Kinematic distributions of leptons in the $H \to ZZ \to 4\ell$ decays of a Higgs boson, $m_H = 125$ GeV: (a) pseudo-rapidity of the highest-$|\eta|$ lepton (the highlighted area corresponds to $|\eta| < 2.4$); (b) transverse momenta of leptons, ranked by their $p_{\rm T}$, in events with all four leptons having $|\eta| < 2.4$ (the hatched areas correspond to $p_{\rm T} > 5$ GeV). These distributions do not include experimental reconstruction efficiencies.

It was also important to achieve a high lepton-$p_{\rm T}$ resolution, which defined the observable four-lepton mass peak width and, hence, had a direct impact on the Higgs boson discovery sensitivity and on measurements of the discovered boson's properties. Typical lepton-$p_{\rm T}$ resolutions achieved by ATLAS and CMS were around 1–2% for $p_{\rm T} \lesssim 100$ GeV. Such resolutions implied that the width of the observable four-lepton mass peak for a SM Higgs boson with $m_H < 300$ GeV would be still defined by the instrumental resolution, while for larger masses by the Higgs boson's natural width. As an example, Fig. 5.2 (b) shows the electron E_T resolution achieved by CMS.

2.2. *Photons*

A few percent of the four-lepton events were expected to have a reconstructible final-state radiation (FSR) photon emitted by one of the leptons. When identified, such photons were included in the calculation of the Higgs boson candidate mass.

Generally, an FSR photon is expected to be soft and nearly collinear to the emitting lepton. Reconstruction of photons with $E_{\rm T}$ in the $1-4$ GeV range and with small angular separation to leptons was yet another

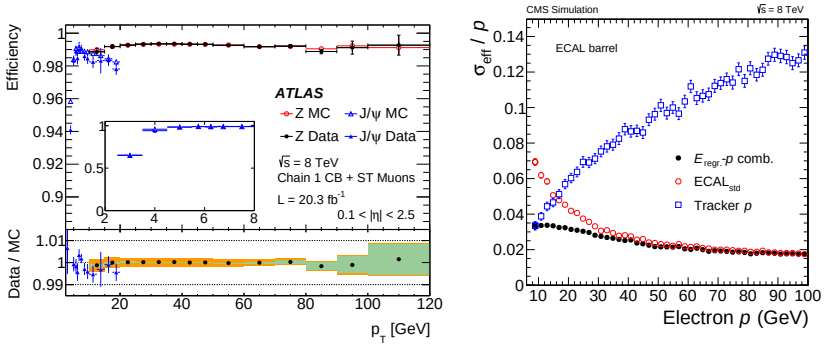

(a) (b)

Fig. 5.2. (a) Muon reconstruction efficiency as a function of p_{T} obtained with the tag-and-probe method applied to the J/ψ and Z resonances (ATLAS). (b) Electron relative E_T resolution as a function of the electron's energy as predicted by simulation (CMS). Contributions of the track's momentum end electromagnetic cluster's energy measurements are also indicated.

feature specific to this analysis. Such low E_{T} thresholds were driven by the experimental four-lepton invariant mass resolution: not accounting for an FSR photon with E_{T} of few GeV would result in mismeasuring the mass of a Higgs boson candidate by more than $1-2\%$ and, consequently, removing it from the signal peak.

The main challenge in FSR photon recovery was to keep a high efficiency of recovering genuine FSR photons and a high rejection factor for abundant unwanted photons mostly coming from π^0 decays. Since only a small fraction of events had reconstructible FSR, the net gain in sensitivity from the FSR photon recovery was $\mathcal{O}(1\%)$. Nevertheless, given the small expected signal yield, both ATLAS and CMS opted for recovering FSR photons in order to make the best use of every single event.

2.3. *Jets*

Both ATLAS and CMS used jets to gain sensitivities to vector boson fusion (VBF) and associated (VH) production. Jets were reconstructed using the anti-k_{T} algorithm, discussed in Chapter **??**, with the clustering distance parameter $D = 0.4$ for ATLAS and 0.5 for CMS. In the case of ATLAS, jets were considered in the analysis only if they had pseudorapdity $|\eta| < 2.5$ and $p_{\mathrm{T}} > 25$ GeV or pseudorapdity $2.5 < |\eta| < 4.5$ and $p_{\mathrm{T}} > 30$ GeV. CMS considered jets with $p_{\mathrm{T}} > 30$ GeV in the pseudorapdity range of $|\eta| < 4.7$.

3. Background processes

Broadly speaking, all four-lepton backgrounds can be classified as either "irreducible" with four prompt leptons not directly associated with jets (hence, very similar to leptons from Higgs boson decays) or "reducible" with one or more leptons, real or fake, closely associated with jets. This association of leptons with jets allows one to suppress, or reduce, the latter backgrounds by very large factors, hence the name "reducible".

Feynman diagrams for the main contributions to "irreducible" background are shown in Fig. 5.3. Figure 5.4 presents the four-lepton mass distributions for each of these contributions.

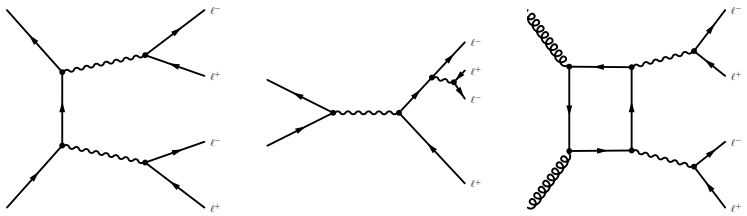

(a) $q\bar{q} \to ZZ \to 4\ell$ (b) $q\bar{q} \to Z \to 4\ell$ (c) $gg \to ZZ \to 4\ell$

Fig. 5.3. The main production modes of "irreducible" background $pp \to 4\ell$ search: (a) and (b) show LO diagrams for $q\bar{q} \to 4\ell$, while (c) shows NNLO diagram of $gg \to 4\ell$. NLO processes are not shown.

The mass distribution for events produced via t-channel $q\bar{q} \to ZZ \to 4\ell$, shown in light blue in Fig. 5.4, has three characteristic regions. For $m_{4\ell} \ll$100 GeV, both propagators shown in Fig. 5.3(a), are predominantly γ^* ($q\bar{q} \to \gamma^*\gamma^* \to 4\ell$) and the cross section nearly diverges as $m_{4\ell}$ goes to zero. For $m_{4\ell} \approx 100$ GeV, the cross section exhibits a step increase as one of the two propagators becomes predominantly an on-shell Z boson, while the other one still has to be γ^*: $q\bar{q} \to Z\gamma^* \to 4\ell$. Near 200 GeV, there is another step increase in cross section as both propagators become predominantly on-shell Z bosons: $q\bar{q} \to ZZ \to 4\ell$. The s-channel $q\bar{q} \to Z \to 4\ell$ decays, shown in Fig. 5.3(b), form a $m_{4\ell}$ peak at the Z boson mass (dark blue in Fig. 5.4) with negligible spillover into the search region with $m_{4\ell} > 110$ GeV.

The NLO corrections to the t- and s-channels include $q\bar{q} \to 4\ell + g$, $qg \to 4\ell + q$, and interference of NNLO $q\bar{q} \to ZZ$ with LO $q\bar{q} \to ZZ$. They add about 30% to the LO cross section and are shown in yellow in Fig. 5.4 (mind the logarithmic scale). The NNLO $gg \to ZZ \to 4\ell$ process, shown

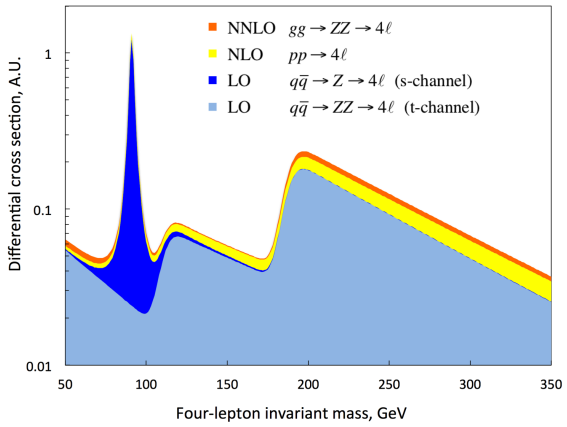

Fig. 5.4. Four-lepton mass distribution for events associated with "irreducible" background $pp \to 4\ell$, obtained at generator-level. Leptons are required to have $p_{\mathrm{T}} > 5$ GeV and $|\eta| < 2.5$, while the invariant mass of opposite-sign dileptons has to be greater than 12 GeV. The following contributions are identified by color and stacked on the plot: LO processes $q\bar{q} \to ZZ \to 4\ell$ (t-channel) and $q\bar{q} \to Z \to 4\ell$ (s-channel); NLO correction to these two LO processes; NNLO process $gg \to ZZ \to 4\ell$.

in (Fig. 5.3(c)), contributes about 10% with respect to the NLO $pp \to 4\ell$ production for $m_{4\ell} > 200$ GeV. However, for four-lepton mass near 125 GeV, this process has a negligible contribution, since diagrams with various quarks in the loop of the $gg \to$ box $\to Z\gamma^*$ process have many partial cancellations arising from sign flips of Z boson and γ couplings to left/right and up/down-type quarks. For $gg \to$ box $\to ZZ$ and $gg \to$ box $\to \gamma^*\gamma^*$, there are no such cancellations as the Z boson and γ^* couplings to the quarks in the loop are effectively squared.

The main sources of the so-called "reducible" background are $Z +$ jets (including heavy flavour quark jets) and $t\bar{t} \to WW + 2\,b-$jets, both giving rise to two prompt and two non-prompt leptons. There is also a contribution from backgrounds with three prompt and one non-prompt leptons: $WZ +$jets and $Z\gamma +$jets (where the photon converts in an electron-positron pair in the detector volume and is misidentified as a prompt electron). After applying all selection requirements, the sum of all "reducible" backgrounds was assessed by ATLAS and CMS from data and found to contribute about $30 - 40\%$ with respect to "irreducible" background in the four-lepton mass range $100 - 180$ GeV and much less at higher masses.

4. Event selection and categorization

ATLAS datasets certified as taken during periods of nominal detector operation and usable for the $H \to ZZ \to 4\ell$ analyses corresponded to an integrated luminosity of 20.3 fb^{-1} at $\sqrt{s} = 8$ TeV and 4.5 fb^{-1} at $\sqrt{s} = 7$ TeV. The corresponding numbers for CMS were 19.6 and 5.1 fb^{-1}.

Both single-lepton and di-lepton triggers were used for online event selection by ATLAS and CMS. CMS also used a tri-electron trigger for the $4e$ case. The trigger efficiency for a signal with respect to the offline selection, described below, was $97 - 100\%$, depending on the final state and the assumed Higgs boson mass in the range $100 - 1000$ GeV.

4.1. *Event selection*

For an event to be selected in the offline analysis, it had to contain at least two pairs of same-flavour and opposite-charge leptons: $e^+e^-e^+e^-$, $\mu^+\mu^-\mu^+\mu^-$ or $e^+e^-\mu^+\mu^-$. The leptons had to satisfy the criteria listed in Table 5.1, which were defined through simulation-based optimizations maximising the *expected* search sensitivity (exclusion limits). ATLAS and CMS, in general, arrived to very similar requirements; however, there were some variations as well. In some cases, these variations were a result of differences in the detector designs and performance, while in other cases the optimal selection criteria had fairly broad ranges so that seemingly different values of requirements resulted in nearly identical expected search sensitivities. Also, as often happens, the same ultimate objectives could be achieved by somewhat different means.

The pseudorapidity requirements on leptons, $|\eta|^{\max}$, were set by the detectors' geometrical acceptance. The minimal p_{T} requirements on leptons, $p_{\mathrm{T}}^{\min}$, were a matter of careful optimization. As discussed in Sec. 2, reconstruction of low-p_{T} leptons was crucial for gaining signal efficiency for a low-mass Higgs boson. However, one also had to worry about the quickly rising rate of "reducible" backgrounds with low-p_{T} "fake" leptons and, also, about reliable measurements of lepton reconstruction efficiencies quickly falling below $p_{\mathrm{T}} \sim 5$ GeV for muons and 10 GeV for electrons.

The isolation requirements on the amount of hadronic energy flowing around leptons were the primary tool for suppressing the reducible backgrounds with non-prompt leptons originating from jets (see Sec 3). ATLAS used tracker-based and calorimeter-based isolations, which were partially correlated as charged hadrons contributed to both. The relative

Table 5.1. Four-lepton event selection criteria in the ATLAS and CMS analyses. SF and DF stand for same-flavour (ee or $\mu\mu$) and different-flavour ($e\mu$) lepton pairings, respectively. The $m_{Z2}^{\min}$ cut in ATLAS is 12 GeV for m_H<140 GeV, rose linearly to 50 GeV at m_H>190 GeV, and then stayed constant for searches of a Higgs boson with higher masses.

Observables	ATLAS	CMS
Leptons:		
electron $\|\eta\|^{\max}$	2.47	2.5
muon $\|\eta\|^{\max}$	2.7	2.4
electron $p_{\mathrm{T}}^{\min}$ (GeV)	7	7
muon $p_{\mathrm{T}}^{\min}$ (GeV)	6	5
maximum relative isolation energy (see text)	0.2–0.3 ($\Delta R = 0.2$)	0.4 ($\Delta R = 0.4$)
maximum impact parameter significance $\|d\|/\sigma$	3.5(μ), 6.5(e)	4.0
$1^{\mathrm{st}}/2^{\mathrm{nd}}/3^{\mathrm{rd}}$ leading lepton $p_{\mathrm{T}}^{\min}$ (GeV)	20/15/10	20/10/-
Di-leptons:		
$\Delta R^{\min}$ (SF/DF)	0.1/0.2	0.02/0.05
invariant mass of Z_1 pair, m_{Z_1} (GeV)	50–106	40–120
invariant mass of Z_2 pair, m_{Z_2} (GeV)	$m_{Z_2}^{\min}$–115	12–120
$m_{\ell^+\ell^-}^{\min}$ (GeV)	5 (SF)	4

tracker-based isolation, defined as the sum of the transverse momenta of all tracks, excluding those associated with leptons of interest, inside a cone of $\Delta R = \sqrt{\Delta\phi^2 + \Delta\eta^2} < 0.2$ around a lepton, divided by the lepton's E_{T}, had to be smaller than 0.15. The relative calorimeter-based isolation, defined as a sum of energy deposits in the electromagnetic and hadronic calorimeters, excluding the lepton's calorimetric footprint, in a cone of $\Delta R < 0.2$ around the lepton, divided by lepton's E_{T}, was required to be smaller than 0.3 for muons and 0.2 (0.3) for electrons in 8 TeV (7 TeV) datasets. CMS used a particle flow algorithm,[14] in which all tracks and all electromagnetic/hadronic calorimeter deposits were grouped to form mutually exclusive "particles" of five kinds: electrons, muons, photons, charged and neutral hadrons. To quantify the amount of energy flowing around a given lepton, the transverse energy of all such particles in a cone $\Delta R < 0.4$ around a lepton was calculated and the ratio of this energy over the lepton's E_{T} was required to be less than 0.4. To maintain the same isolation requirement efficiency for different pileup conditions (and hence minimize potential systematic uncertainties), both ATLAS and CMS used isolation energy corrections calculated on the per-event basis as a function of the number of vertices found and the average amount of transverse energy flowing in the event.

Rejecting leptons not pointing to the primary vertex was another handle to suppress non-prompt leptons originating from long-lived hadrons,

such as B mesons, or electrons originating from photon conversions in the beam pipe and detector material. ATLAS discarded muons (electrons), if their impact parameter in the transverse plane divided by its estimated measurement uncertainty, $|d|/\sigma$, was greater than 3.5 (6.5). CMS used a 3D-impact parameter, the closest distance between the track helix and the event primary vertex, and discarded leptons with $|d|/\sigma > 4$.

Requirements on the transverse momentum, p_{T} of the two leading leptons (20 and 15 GeV for ATLAS, 20 and 10 GeV for CMS) ensured that selected events had a high trigger efficiency and, hence, known with small uncertainties.

Leptons were required to be separated from each-other by a minimum ΔR^{min} distance. The primary purpose of this requirement was to reject rare occasions of duplicates when one lepton was reconstructed as two. Whenever this happened, the original and "fake" leptons would tend to be nearly collinear.

In the decays of a Higgs boson with a mass in the range 110–180 GeV, one Z boson is expected to be mostly on-shell, while the other off-shell. Therefore, between four leptons in an event, the pair of opposite-sign same-flavour leptons with its invariant mass closest to the Z boson mass, to be denoted henceforth as Z_1, was required to have its mass in the range 50–106 GeV for ATLAS and 40–120 GeV for CMS. The m_{Z_1} cuts had a very high efficiency for a signal and helped reduce backgrounds without Z bosons, such as $t\bar{t}$ and $WW + jets$. The low-end cut on m_{Z_1} was as low as 40 or 50 GeV in order to keep a high acceptance for a low-mass Higgs boson occasionally decaying into two off-shell Z bosons: $H \to Z^*Z^* \to 4\ell$.

The low-end cut on the invariant mass of the remaining pair[‡], denoted as Z_2, was a subject of detailed optimizations. Lowering this requirement would naturally increase the signal efficiency for a low-mass Higgs boson. However, the rate of backgrounds, including the "irreducible" background $q\bar{q} \to Z(Z^*/\gamma^*) \to 4\ell$ would grow as well. Both ATLAS and CMS arrived to a conclusion that the cut near 12 GeV would be close to optimal for the low-mass Higgs boson searches ($m_H < 140$ GeV). In a search for a Higgs boson of higher masses, the cut could be raised, as was done by ATLAS (see Table 5.1). CMS refrained from varying the cut value, as the expected sensitivity gains were considered to be small. The upper cut on m_{Z_2}, 115 or 120 GeV, was not consequential and was added as a safe-guard against non-ZZ background.

[‡]The subtleties of selecting a Z_2 pair in rare events with more than four leptons can be found in the original papers.

Finally, the cut $m^{\min}_{\ell^+\ell^-} > 5/4$ GeV (ATLAS/CMS) on all same-flavour lepton pairs helped suppress background $q\bar{q} \to \gamma^*\gamma^* \to (\ell^+\ell^-)(\ell^+\ell^-)$. The cross section for this background rises fast as m_{γ^*} decreases. The potential danger was that such events with two γ^*'s of low mass and high $p_{\rm T}$ might nevertheless pass the selection criteria should the Z_1 and Z_2 pairs be formed from leptons associated with different γ^*'s. CMS decided to extend the $m^{\min}_{\ell^+\ell^-}$ cut to include lepton pairs of different flavour, motivated by considering backgrounds with 2 b-quark jets, e.g.: $pp \to b\bar{b} \to (e^+\mu^- + X)(e^-\mu^+ + X)$. Again, same-flavour lepton pairs might pass the m_{Z_1} and m_{Z_2} cuts, but would fail the $m^{\min}_{e^\pm\mu^\mp}$ cut as $e^\pm\mu^\mp$ pairs in such events would come from B mesons with a mass of about 5 GeV.

The signal efficiency, which includes the detector acceptance, lepton reconstruction efficiency, and efficiency of event selection requirements, is shown in Fig. 5.5. The difference between efficiencies for the three final state was due to the lower reconstruction efficiency for electrons in comparison to muons. The overall decline of efficiency at lower Higgs boson masses was due to smaller efficiency for low $p_{\rm T}$ leptons (acceptance, reconstruction, and isolation) and falling efficiency of the low-end m_{Z2} cut.

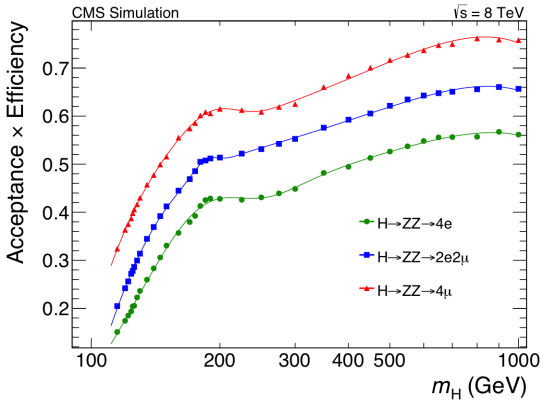

Fig. 5.5. Four-lepton event acceptance times reconstruction/selection efficiency as a function of the Higgs boson mass for CMS in the 8 TeV dataset. Efficiencies for different final states are shown separately.

Table 5.2 shows the expected and observed event yields after all selection requirements in the wide range of four-lepton masses as well as for a narrow range around 125 GeV. For simplicity, all four-lepton final states are summed.

Table 5.2. Expected and observed numbers of events in two four-lepton mass ranges: $m_{4\ell} > 100$ GeV and in 10/9 GeV windows near 125 GeV. The assumed SM Higgs boson mass is 125 GeV. The numbers in parentheses are not given in the original publications; they are estimates made by the authors of this chapter.

	ATLAS		CMS	
	>110 GeV	120–130 GeV	>100 GeV	121.5–130.5 GeV
"irreducible" background	381 ± 20	7.41 ± 0.40	387 ± 31	6.8 ± 0.3
"reducible" background	18.9 ± 2.4	2.95 ± 0.33	22.6 ± 3.6	2.6 ± 0.4
$H \to ZZ \to 4\ell$	18.2 ± 1.8	16.2 ± 1.6	(19)	17.3 ± 1.3
total expected	418 ± 20	26.5 ± 1.7	(429 ± 31)	26.7 ± 1.4
observed	466	37	470	25

4.2. *Recovery of final state radiation*

Both ATLAS and CMS searched for FSR photons (see Sec. 2.2) and, when identified, included them in the Higgs boson candidate mass calculation. FSR photons have a spectrum $dN/dE_\gamma \sim 1/E_\gamma$ and tend to be emitted along leptons. Considering this, ATLAS defined "collinear" FSR candidates ($\Delta R_{\ell\gamma} < 0.15$ and $E_T^\gamma > 1.5$ GeV) and "non-collinear" FSR candidates ($\Delta R_{\ell\gamma} > 0.15$ and $E_T^\gamma > 10$ GeV). CMS definitions for FSR candidates were as follows: "collinear", if $\Delta R_{\ell\gamma} < 0.07$ and $E_T^\gamma > 2$ GeV, and "non-collinear", if $0.07 < \Delta R_{\ell\gamma} < 0.5$ and $E_T^\gamma > 4$ GeV. To be included in calculation of the mass, an FSR photon candidate had to be isolated and was required to bring the invariant mass of $\ell^+\ell^-\gamma$ closer to the Z boson mass in comparison to the $\ell^+\ell^-$ mass. In ATLAS, the FSR recovery procedure was applied to leptons in the leading Z_1 pair only, while in CMS—for all leptons.

On average, about 5% of four-lepton events were FSR-corrected. The estimated efficiency of the procedure was about 50–70%, with respect to the number of true FSR photons with the same ΔR and E_T^γ requirements. The purity was estimated to be between 80–95%, i.e. 5–20% of photons identified as FSR were actually not FSR photons. The FSR recovery procedure was validated by applying it to $Z \to \ell^+\ell^-$ decay. FSR photons were found in a few percent of Z boson decays, in agreement with expectations, and the reconstructed invariant mass of the $\ell^+\ell^-\gamma$ system for such events formed a much improved peak around the Z boson mass.

4.3. *Event categorization*

Selected events were classified into categories, aiming to improve search and measurement sensitivities, to facilitate studies of various signal properties, and help with analysis flow book-keeping.

4.3.1. *Categorization by centre-of-mass energy*

Both ATLAS and CMS treated events from the $\sqrt{s}$ =7 and 8 TeV datasets separately. This simplified the basic analysis bookkeeping (run conditions, calibrations, simulation samples, etc.).

4.3.2. *Categorization by flavour of the four-lepton system*

CMS used three lepton-flavour-dependent event categories: $4e$, 4μ, $2e2\mu$. Keeping events of different expected signal-to-background ratio in separate groups helped to maximise the overall search and measurement sensitivities. In comparison to the $4e$ final state, 4μ events were expected to have a higher signal-to-background ratio due to better four-lepton mass resolution (see Figs. 5.6 and 5.7) and smaller "reducible" backgrounds (see Sec. 6). In terms of the signal-to-background ratio, the $2e2\mu$ event category was in between.

	$4e$	$2e2\mu/2\mu2e$	4μ
ATLAS	2.2	1.8	1.6
CMS	2.0	1.6	1.2

Fig. 5.6. Four-lepton mass resolution in GeV (σ of the Gaussian core) for a 125 GeV Higgs boson.

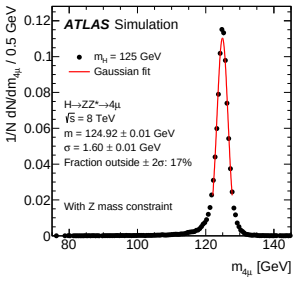

Fig. 5.7. Simulated four-muon invariant mass distributions for $H \to ZZ \to 4\mu$ (ATLAS).

ATLAS divided $2e2\mu$ events further into two separate categories, $2e2\mu$ and $2\mu2e$, depending on whether $2e$ or 2μ pair would be counted as Z_1. For events with $m_{4\ell} < 2\,m_Z$, the Z_1 pair would contribute the most to the four-lepton mass and, hence, $2\mu2e$ events were expected to have a better average mass resolution than $2e2\mu$ events. On the other hand, $2\mu2e$ events

with low p_{T} electrons associated with the Z_2 pair were expected to have a higher relative contribution of "reducible" background in comparison to $2e2\mu$ events, since soft electrons are easier to fake. The two trends, however, had opposite effects on the signal-to-background ratio and largely compensated each other so that the net gain in sensitivities from splitting events with dilepton pairs of different flavours into $2e2\mu$ and $2\mu2e$ categories was found to be relatively small.

4.3.3. *Categorization by production mechanism signatures*

To probe different Higgs boson production mechanisms, ATLAS and CMS introduced production-mechanism-sensitive categories. ATLAS used four categories (dijet VBF, dijet VH, leptonic VH, and untagged), while CMS used only two categories (dijet and untagged).

The categorisation employed by ATLAS was as follows. If an event had at least two jets and the two highest p_{T} jets (two "leading" jets) had an invariant mass $m_{jj} > 130$ GeV, the event was assigned to the VBF-tagged category. If $40 < m_{jj} < 130$ GeV and a dedicated multivariate-observable trained using a Boosted Decision Tree algorithm (BDT - see Appendix **??**) $\mathrm{BDT_{VH}} > -0.4$, such an event would be assigned to the dijet VH-tagged category. The $\mathrm{BDT_{VH}}$ was trained to separate VH from gluon-gluon fusion production using the following five inputs: m_{jj}, p_{T} of each of the two leading jets, pseudorapidity of the highest p_{T} jet, and absolute value of the difference between two leading-jet pseudorapidities $|\Delta\eta_{jj}|$. From the remaining events, those with at least one additional (i.e. fifth) lepton with $p_{\mathrm{T}} > 8$ GeV would form the leptonic VH category. The untagged category comprised all remaining events.

In the CMS categorisation scheme, events with two or more jets were assigned to the dijet category and all other events to the untagged category.

Table 5.3 lists the expected and observed event counts in each of the production mechanism categories. Note that VBF and VH categories are expected to contain a substantial fraction of signal events produced via gluon-gluon fusion. In comparison to the untagged category, VBF and VH categories were expected to have better signal-to-background ratio, albeit with considerably smaller event yields.

Table 5.3. Expected and observed event counts in each of the production mechanism tag categories. ATLAS (CMS) results are for four-lepton mass range 120–130 (121.5-130.5) GeV and for an assumed Higgs boson mass of 125 (126) GeV.

		gF+ttH+bbH	VBF	VH	total H	total bkg	observed
ATLAS	untagged	12.8	0.57	0.35	13.7	9.8	34
	dijet VBF	1.18	0.75	0.10	2.03	0.42	3
	dijet VH	0.40	0.03	0.21	0.64	0.18	0
	leptonic VH	0.013	<0.001	0.069	0.082	0.031	0
CMS	untagged	15.4	0.70	0.49	16.6	8.5	20
	dijet	1.7	0.87	0.37	3.0	0.9	5

5. Continuous observables

The four-lepton events were further characterised by introducing observables that helped enhance search and measurement sensitivities, but were not used for explicit cuts. Instead, the analyses took into account entire shapes of their distributions, which allowed for using maximally the discriminating information carried by these observables. In this section, we describe such observables that were selectively used in different sub-analyses to be presented in Sections 7 – 11. Observables specific to measurements of the discovered boson's mass, total width via its far off-shell production, and studies of spin-parity properties are described in the corresponding sections.

5.1. *Four-lepton invariant mass*

The four-lepton invariant mass was the prime shape observable. The SM Higgs boson events were expected to form a distinct resonance peak not characteristic of any background. As mentioned earlier, for $m_H < 300$ GeV, the intrinsic width of the SM Higgs boson is smaller than the instrumental four-lepton mass resolution. Whenever an FSR photon was identified, it was added to the calculation of the mass. ATLAS improved the average $m_{4\ell}$ resolution by about 15% by refitting the invariant mass of each four-lepton event with Z-mass constraints, on the Z_1-pair mass for events with $m_{4\ell} < 190$ GeV and both Z_1 and Z_2 pair masses for events with $m_{4\ell} > 190$ GeV, in which both Z bosons would tend to be produced on-shell. The fit was taking into account the Z boson line-shape, the reconstructed dilepton mass and its instrumental uncertainty.

Figure 5.8 shows the four-lepton invariant mass distributions (separately

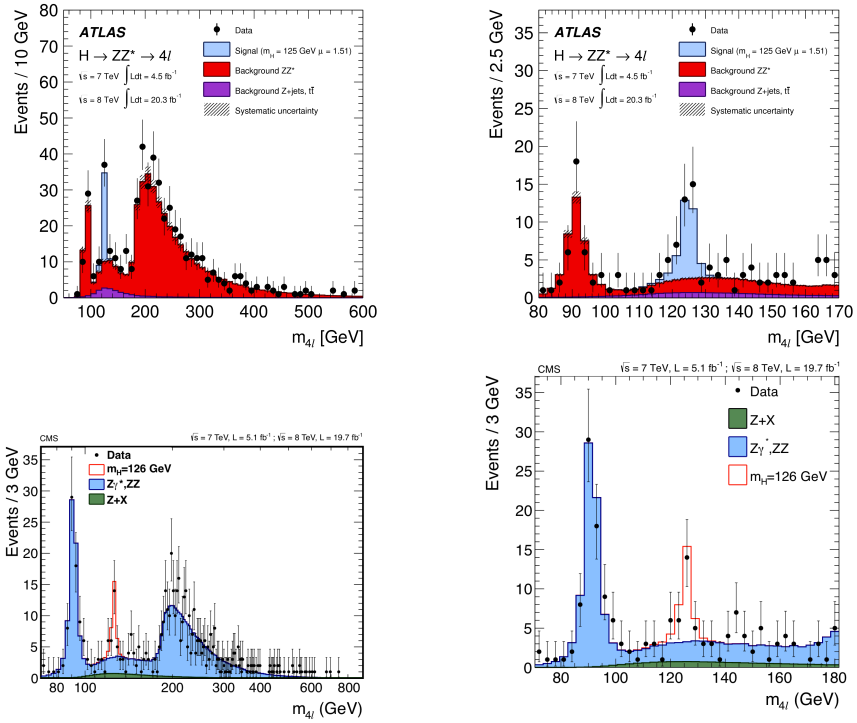

Fig. 5.8. Four-lepton invariant mass distributions for ATLAS (top) and CMS (bottom) data in the full mass range (left) and the low-mass range (right). Data are shown as points. The background contributions along with the expectation for the SM Higgs boson production are shown as histograms. For ATLAS, the expectations for SM Higgs boson with $m_{\mathrm{H}} = 125$ GeV are scaled up by factor 1.51, the best-fit signal strength obtained in data.

for the full and the low-mass ranges) for all events passing the selection criteria. In this and following figures, events of all four-lepton final states and data from the 7 TeV and 8 TeV runs are shown together, although, in the actual analyses, events of different event categories were always analysed separately. In the low-mass range, signal-like peaks near 125 GeV are visually evident in both ATLAS and CMS data without any formal statistical analysis. Outside the 125 GeV peak region, the distributions were consistent with the expected background. The peak at $m_{4\ell} \sim m_Z$ corresponds to $Z \to 4\ell$ decays (Fig. 5.3(b)); it is more pronounced in CMS data owing to the lower p_{T} cuts.

5.2. *Four-lepton kinematic discriminants*

To help separate signal from background, ATLAS and CMS made use of kinematic discriminants calculated for each four-lepton event as the ratio of leading-order matrix elements, $\mathcal{A}_{\rm H}(\mathcal{P})$ for the $gg \to H \to 4\ell$ signal, and $\mathcal{A}_{\rm ZZ}(\mathcal{P})$ for the prevailing $q\bar{q} \to ZZ \to 4\ell$ background:

$$d = \frac{|\mathcal{A}_{\rm H}(\mathcal{P})|^2}{|\mathcal{A}_{\rm ZZ}(\mathcal{P})|^2}, \tag{5.1}$$

where $\mathcal{P}$ stands for momenta of the four final-state leptons. The signal matrix element $\mathcal{A}_{\rm H}$ was calculated assuming $m_H = m_{4\ell}$; hence, the observable d discriminated on the basis of a kinematic configuration of four leptons in an event, rather than on the four-lepton invariant mass. Matrix elements were calculated and cross-validated by using a number of tools,[15–22] including various event generators, exact for any four-lepton final state, and explicit analytic formulas, which were available for the $2e2\mu$ final state only[§].

In the mass range near 125 GeV, using the matrix-element-based discriminant boosted the Higgs boson search sensitivity by about 20%. This discrimination power arises mostly from the m_{Z_2} mass distribution differences:[18] for a signal, the Z_2 pair is always produced via off-shell Z boson and tends to "prefer" the highest possible mass, while for background, dominated in the low four-lepton mass range by $q\bar{q} \to Z\gamma^* \to (\ell^+\ell^-)(\ell^+\ell^-)$, this lepton pair is expected to "prefer" lower invariant masses. Also, the low mass tail of the m_{Z_1} distribution is expected to be less suppressed for Higgs boson events. When Z_1 goes off-shell ($m_{Z_1} < m_Z$), the suppression is partially compensated by allowing for m_{Z_2} to get closer to m_Z. Figure 5.9 shows the m_{Z_1} and m_{Z_2} distributions for events in the 125 GeV peak. Indeed, the excess events revealed the expected pattern.

For the purposes of technical convenience, the discriminant d was monotonically transformed[¶]. ATLAS simply used $D_{ZZ^*} = \log(d)$. CMS transformed the discriminant d so that the new one, denoted as $D^{\rm kin}_{\rm bkg}$, would range between 0 and 1: $D^{\rm kin}_{\rm bkg} = [1 + c_{m_{4\ell}} \cdot d]^{-1}$, where an ad-hoc constant $c_{m_{4\ell}}$ was adjusted for each bin of $m_{4\ell}$ in order to prevent distributions from being too compressed against 0 or 1.

[§]The case of the $4e$ and 4μ states is more complicated due to interference associated with permutations of identical leptons, which is particularly pronounced for events with off-shell Z bosons.

[¶]Monotonic transformations do not change the discrimination power of observables as they do not change relative ranking of events.

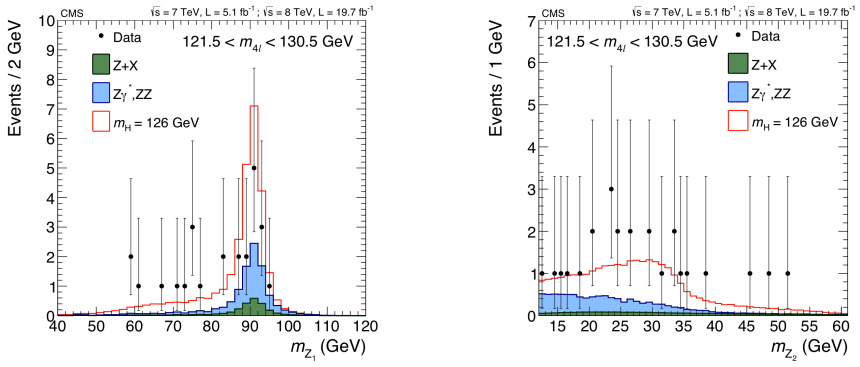

(a) (b)

Fig. 5.9. Dilepton mass distributions for events with $121.5 < m_{4\ell} < 130.5$ GeV, as obtained by CMS: (a) m_{Z_1} for the pair of leptons of same flavour and opposite charge with their invariant mass closest to m_Z, (b) m_{Z_2} for the remaining pair.

Matrix elements calculated at LO are oblivious of the four-lepton event transverse momentum $p_{\mathrm{T}}^{4\ell}$ (NLO effect) or its rapidity $y^{4\ell}$ (PDF and NLO effects). However, these observables carry some signal-vs-background separation. Since the initial state radiation from gluons is more prolific than from quarks, the four-lepton system tends to have higher transverse momentum for signal ($gg \to H \to 4\ell$) than for ZZ background ($q\bar{q} \to ZZ \to 4\ell$). Also, the four-lepton system produced in $q\bar{q} \to ZZ \to 4\ell$ process tends to be more boosted along the beam line due to very different quark and anti-quark parton density functions. ATLAS exploited these features by introducing a multivariate observable, BDT_{ZZ^*}, trained using three inputs: matrix-element discriminant D_{ZZ^*}, four-lepton transverse momentum $p_T^{4\ell}$, and four-lepton pseudorapidity $\eta^{4\ell}$. CMS also used $p_T^{4\ell}$, but kept it as an independent observable, aiming both to help separate signal from ZZ background as described above and to attain some sensitivity to the VBF+VH production component of the untagged event category. A Higgs boson produced in VBF or VH processes recoils already at LO against either two quarks or a W/Z boson, which leads to higher Higgs boson transverse momenta in comparison to the case of gluon-gluon fusion process. However, quantitative studies showed that gains in Higgs boson discovery sensitivity from using the four-lepton transverse momentum and rapidity observables were rather small, at the level of $\mathcal{O}(1\%)$.

Figures 5.10(a) and 5.10(b) show the $\mathrm{BDT}_{\mathrm{ZZ}^*}$ (ATLAS) and $D_{\mathrm{bkg}}^{\mathrm{kin}}$

(CMS) distributions for events with $m_{4\ell}$ near 125 GeV. The expected distributions, shown by histograms, demonstrate a clear separation between the SM Higgs boson and the dominant $q\bar{q} \to ZZ$ background. Also, one can see that the observed events are skewed to the right, as one would expect in a presence of a Higgs boson signal.

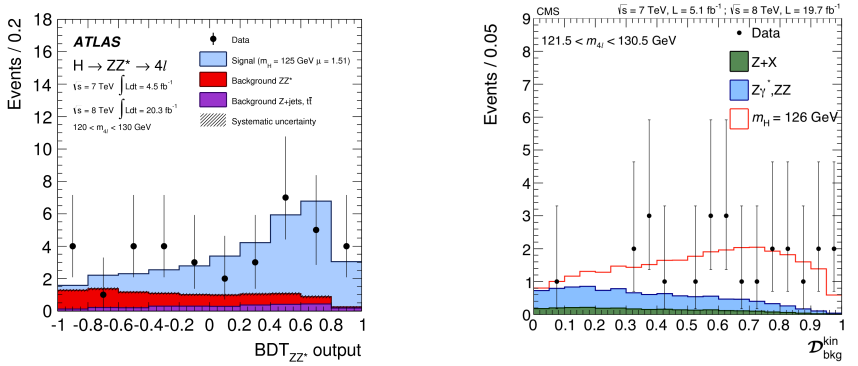

(a) (b)

Fig. 5.10. (a) Discriminant $\mathrm{BDT_{ZZ^*}}$ distribution for events with four-lepton invariant mass in the range 120–130 GeV (ATLAS). (b) Discriminant $D^{\mathrm{kin}}_{\mathrm{bkg}}$ distribution for events with four-lepton invariant mass in the range 121.5–130.5 GeV (CMS).

5.3. *Di-jet discriminant*

The di-jet tagged category was enriched in signal events; nevertheless, it still contained a large fraction of $gg \to H$ signal events and background as well. The large rapidity distance between two leading jets $|\Delta\eta_{jj}|$ and their invariant mass m_{jj} were both used to help distinguish signal events produced via VBF mechanism from gluon-gluon fusion. However, these two observables had a strong correlation. CMS consolidated them into one VBF discriminant $D_{jet} = \alpha\,|\Delta\eta_{jj}| + \beta\, m_{jj}$, where α and β coefficients were optimised to provide the maximum discrimination power between VBF and gluon fusion production mechanisms. Such a linear construct is known as a Fisher discriminant. ATLAS trained an MVA-observable $\mathrm{BDT_{VBF}}$ using the following five inputs: m_{jj}, $|\Delta\eta_{jj}|$, p_{T} of each of the two leading jets, and the pseudorapidity of the leading jet. The VBF discriminants were also efficient in separating the VBF produced Higgs boson signal events in the VBF di-jet category from the background, thus improving the overall

signal sensitivity.

ATLAS and CMS observed three and five events, respectively, in their VBF di-jet categories with $m_{4\ell} \sim 125$ GeV. One ATLAS event had Higgs signal to ZZ background ratio of about 6, and 60% probability to arise from VBF production, still very modest for any affirmative claims. The VBF purity of all five CMS events was smaller.

6. Signal and background modelling

The signal and background modelling, including the assessment of associated systematic uncertainties, was evolving over time. The description presented in this chapter is based on the final analyses published with the full Run 1 dataset. The tools and methods used by ATLAS and CMS in setting up their models were very similar.

6.1. *Processes with four prompt leptons*

The processes with four prompt leptons were modelled using simulation. Particle-level events were simulated using appropriate event generators as shown in Table 5.4. The best-known cross sections were used to normalize simulated events to represent the expected event yields for the given integrated luminosity. Signal cross sections were taken from Refs. [3,23] (see Chapter **??** for details). The particle-level events were then processed through the ATLAS and CMS detector simulation, which propagated the generated particles through the detector volume and emulated detector's response. Pile-up pp interactions were added with their multiplicity distributions matched to those observed in data. Then, the simulated detector response was used to reconstruct events with the same algorithms that were used with the data. Finally, the simulation-based signal and background models were corrected for differences between simulated and actual detector performance (lepton reconstruction efficiency, lepton p_{T} scale, lepton p_{T} resolution, jet energy scale, etc.), where the actual detector performance was obtained from dedicated analyses of data, relying on data-driven techniques such as the tag-and-probe method.

Some of the simulated samples were corrected to improve the theoretical accuracy of models implemented in corresponding generators. For example, the POWHEG-generated gluon fusion events were given additional weights so the p_{T} distribution of reweighted events would match the one calculated at the NLO+NNLL level.

Table 5.4. Simulated processes with four prompt leptons. Parton showering and hadronization, including the underlying event, are simulated with PYTHIA for all listed processes. Processes $gg/q\bar{q} \to X$ stand for production of a particle with spin-parity properties different from the SM Higgs boson. Processes marked with "Yes" had additional theory-based corrections applied, as described in the text.

Process	ME generator	Corrections	Cross section
$gg \to H$	POWHEG (NLO)	Yes	$(\text{NNLO} + \text{NNLL})_{\text{QCD}} + \text{NLO}_{\text{EW}}$
VBF	POWHEG (NLO)	Yes	$\text{NNLO}_{\text{QCD}} + \text{NLO}_{\text{EW}}$
WH and ZH	PYTHIA (LO)		$\text{NNLO}_{\text{QCD}} + \text{NLO}_{\text{EW}}$
$t\bar{t}H$	PYTHIA (LO)		NLO_{QCD}
$b\bar{b}H$ (ATLAS)	see text		$\text{NLO}_{\text{QCD(4FS)}} + \text{NNLO}_{\text{QCD(5FS)}}$
$gg/q\bar{q} \to X$	JHUGEN (LO)	Yes	normalized to data
$q\bar{q} \to ZZ$	POWHEG (NLO)		NLO_{QCD}
$gg \to ZZ$	GG2ZZ (LO)		LO and (LO)×K-factor
DPI $(q\bar{q} \to Z) \times 2$	PYTHIA		phenomenological

For a SM Higgs boson with $m_H \gtrsim 400$ GeV, the narrow-width approximation implemented in POWHEG was not adequate. Also, for gluon-gluon fusion the effect of interference between $gg \to H \to ZZ$ and non-resonant $gg \to ZZ$ needed to be accounted for. CMS reweighted the POWHEG samples ($gg \to H$ and VBF) in this mass range to match the Higgs boson mass lineshape calculated in a complex-pole scheme.[24]

Neither POWHEG nor PYTHIA simulated the effects of interference associated with permutations of identical leptons in $H \to ZZ \to 4e$ and 4μ decays, which was important in spin-parity studies.[18] CMS opted to keep Higgs bosons stable in POWHEG $gg \to H$ and VBF samples and perform Higgs bosons' decays with JHUGEN,[15–17] which treated the interference properly. For simulation of $gg \to H$, ATLAS used JHUGEN and reweighted the simulated events to match their p_{T} distribution to the NLO+NNLL calculation.

The small contributions from WH, ZH, and $t\bar{t}H$ processes were simulated with PYTHIA. The SM $b\bar{b}H$ production is expected to contribute less than 1% of the total cross-section. ATLAS included and treated it as a small correction to gluon fusion, while CMS chose to neglect it.

Production of bosons with exotic spin-parity properties was simulated with JHUGEN. In absence of established contender models for such exotic bosons that would predict definitive production cross sections, event yields in those models were set to the number of observed signal events.

Background $q\bar{q} \to ZZ \to 4\ell$ was generated with NLO POWHEG, which

was also used for assessing the process cross section. Background $gg \to ZZ \to 4\ell$ was simulated with GG2ZZ at LO. In analyses probing the Higgs boson off-shell production, where $gg \to ZZ$ background was of high importance, the $gg \to H \to ZZ$ K-factor was used as a proxy[25] for the $gg \to ZZ$ background.

Double-parton interactions (DPI) with two "independent" $q\bar{q} \to Z$ interactions taking place within the same proton-proton collision was simulated with PYTHIA. The overall cross section was assessed from a general phenomenological formula $\sigma_{\rm DPI} = \sigma_1\sigma_2/\sigma_{\rm eff}$, where σ_1 and σ_2 are cross sections for two single parton-parton processes of interest ($q\bar{q} \to Z_1$ and $q\bar{q} \to Z_2$), and $\sigma_{\rm eff}$ is a universal phenomenological parameter measured to be about 15 mb for pp collisions at $\sqrt{s} = 7$ TeV [26]. The DPI background was found to be negligible.

6.2. *Reducible background*

In the mass range 100-180 GeV, "reducible" backgrounds consisting of events with one or two leptons of non-prompt origin were estimated to contribute as much as 30–40% in addition to the "irreducible" background (see Table 5.2). Although the primary processes contributing to "reducible" backgrounds were well known (see Sec. 3), accurate simulation of rare instances of reconstructing objects of non-prompt origin as "tight" leptons was challenging. Here, "tight" refers to the final lepton selection criteria. Objects of non-prompt origin could be a lepton from B hadron decays, an electron originating from a photon conversion, a muon from a pion in-flight decay $\pi \to \mu\nu$, a charged pion faking an electron via the charge-exchange interaction (e.g., $\pi^- p \to \pi^0 n$) in the electromagnetic calorimeter, etc. Probabilities of reconstructing such objects as "tight" leptons, being very small, depended strongly in relative terms on various subtleties of jet fragmentation and particle interactions with the detector, whose accurate modelling was not guaranteed.

Therefore, to predict the net "reducible" background in the signal region, ATLAS and CMS opted for data-driven methods. The method used by ATLAS was based on unravelling the background composition and dealing with each contribution separately, while CMS treated all background sources more inclusively. In the following, we briefly describe the CMS method and then highlight the distinct features of the ATLAS approach.

The CMS method assumed that there were two distinct groups of "reducible" background processes with either two or three prompt leptons,

with the unknown number of events X_2 and X_3 respectively, and that the probability of reconstructing an object of non-prompt origin as a lepton with "tight" and "loose" selection criteria were $\epsilon_{\rm T}$ and $\epsilon_{\rm L}$, respectively. "Loose" selection did not include isolation requirements and certain reconstruction quality criteria. The number of observed events N^{obs}_{CR2} and N^{obs}_{CR3} in two control regions—$CR2$ with two "tight" leptons and two "loose" leptons, failing the "tight" selection criteria, and $CR3$ with three "tight" leptons and one "loose-but-not-tight" lepton—were related to X_2, X_3, $\epsilon_{\rm T}$, and $\epsilon_{\rm L}$ as follows:

$$\begin{aligned} N^{obs}_{CR2} &= X_2 \cdot (\epsilon_{\rm L} - \epsilon_{\rm T})^2 \\ N^{obs}_{CR3} &= X_3 \cdot (\epsilon_{\rm L} - \epsilon_{\rm T}) + X_2 \cdot 2\epsilon_{\rm T}(\epsilon_{\rm L} - \epsilon_{\rm T})\,. \end{aligned}$$

From these two equations, the predicted expected number of "reducible" background events in the signal region ($N_{SR} = X_2 \cdot \epsilon_{\rm T}^2 + X_3 \cdot \epsilon_{\rm T}$) was obtained:

$$N_{SR} = N^{obs}_{CR3} \cdot \frac{\epsilon}{1-\epsilon} - N^{obs}_{CR2} \cdot \left(\frac{\epsilon}{1-\epsilon}\right)^2 , \qquad (5.2)$$

where ϵ is the "tight-to-loose" ratio of two probabilities, $\epsilon = \epsilon_{\rm T}/\epsilon_{\rm L}$, also referred to as a transfer factor. This ratio was measured in control regions of $Z(\ell^+\ell^-) + e/\mu$ events with low missing transverse momentum required in order to suppress WZ events. The non-Z lepton in such events provided a clean source of reconstructed leptons of non-prompt origin.

Potential systematic biases arising from differences in ϵ for different non-prompt objects were minimized by using isolation as the prime difference between "loose" and "tight" leptons and by measuring "tight-to-loose" ratios for electron and muons in bins of $p_{\rm T}$ and η. The validity of this method was confirmed by simulation. With ϵ being a function of $p_{\rm T}$ and η, the two terms in Eq. (5.2) then represent sums of $CR2$ and $CR3$ events reweighted by measured probabilities on an event-by-event basis. The predictions of Eq. (5.2) were obtained in bins of various four-lepton observables used in the $H \to ZZ \to 4\ell$ analyses. The method was validated on data using events with four leptons of wrong charge/flavour combinations ($\mu^+\mu^-\mu^+e^-$, $\mu^+\mu^-e^+e^+$, etc), as shown in Fig. 5.11(a).

In the ATLAS approach, separate analysis schemes were developed for $\ell\ell+\mu\mu$ and $\ell\ell+ee$ events, motivated by the fact that leptons of non-prompt origin were most likely to end up in the Z_2 dilepton pair and that processes leading to "fake" muons and electrons were notably different. Using physics considerations, "reducible" background processes were classified in a few

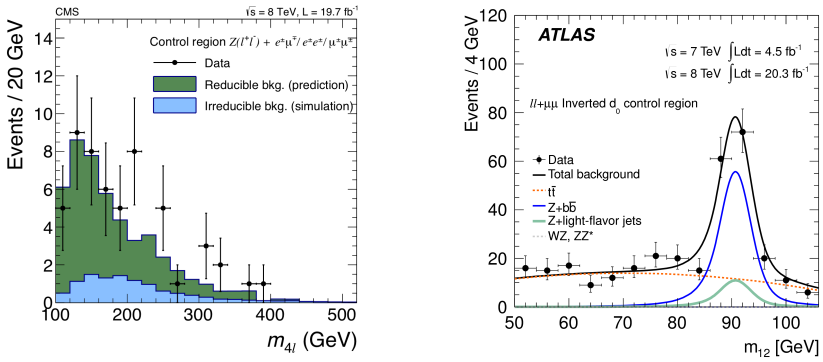

(a) (b)

Fig. 5.11. (a) CMS: Predicted and observed "reducible" background in the control region with four leptons of wrong charge/flavour combinations and passing all "tight" selection requirements (validation of the method). (b) ATLAS: Observed m_{Z_2} mass distribution in one of the four $\ell\ell+\mu\mu$ control regions (see text). The fitted contributions from $t\bar{t}$, $Zb\bar{b}$, and $Z+jets$ are also shown.

groups. Then, a simultaneous fit to observations in several control regions with one or two "loose" leptons, enriched differently by each process, was used to extract the number of events of each type and extrapolated to the signal region, by applying transfer factors tuned for each process.

For $\ell\ell+\mu\mu$, the processes considered were $t\bar{t}$, Zbb, and $Z+jets$ (light quarks and gluons). Four control regions were defined and the fit was performed for the m_{Z_1} distribution in each of them. Figure 5.11(b) shows such a fit in a control region, where both muons from the Z_2 pair were not required to pass isolation cuts and at least one of them had to fail the impact parameter requirement. This control region was expected to be enriched with $t\bar{t}$ and $Zb\bar{b}$, as the fit results indeed confirmed.

For $\ell\ell+ee$, there was one control region with considerably relaxed requirements on the sub-leading p_{T} electron from the Z_2 pair. The processes considered were classified according to the origin of an object potentially faking the "loose" electron: $(\ell\ell+e)$ plus a light-flavour hadron, $(\ell\ell+e)+\gamma$, and $(\ell\ell+e)+b$. The three contributions were disentangled in a fit of events in the 2D-distribution of two observables: the number of track hits in the innermost layer of the pixel detector (electrons induced by conversions often originated past the innermost layers), and the ratio of the number of high-threshold and low-threshold hits in the Transition Radiation Tracker

(for charged hadrons, this ratio tended to be low).

The simulation-based transfer factors for each process were validated/corrected in the analysis of the $Z(\ell^+\ell^-)+\ell$ data, again with selection adjustments enhancing different sources of non-prompt leptons. Results obtained in data agreed well with simulation for all processes with one exception: rates with which charged light hadrons were faking electrons had to be corrected by a p_{T}-dependent factor of $\sim$2.

6.3. *Uncertainties*

Thanks to the narrow Higgs boson width, most of uncertainties in the signal and background models could be effectively treated as uncertainties on the yield of four-lepton events with $m_{4\ell} \approx m_H$. The only important exception is the shape of the four-lepton mass distribution for the signal. Overall, the impact of systematic uncertainties on the final results obtained in the $H \to ZZ \to 4\ell$ channel in Run 1 was marginal.

6.3.1. *Normalization uncertainties*

The normalization uncertainties were assessed as a function of four-lepton mass and separately for each exclusive event category. Uncertainties in different exclusive categories arising from the same source were treated as correlated.

Theoretical uncertainties on the overall signal and irreducible background event yields were of the order of 10% and 5%, respectively. These uncertainties – assessed separately for each contributing process – were either taken explicitly from phenomenological papers or were obtained by following the commonly accepted phenomenological prescriptions: the PDF4LHC recommendation[27] for assessing PDF+α_s related uncertainties, varying QCD renormalisation and factorisation scales by a factor of two, and the Stewart-Tackmann prescription[28] for jet-based categorizations.

The main sources of instrumental uncertainties on the expected event yields for simulated samples (signal and irreducible background) were associated with lepton reconstruction/selection efficiencies. These efficiencies were evaluated using the "tag-and-probe" technique exercised on $Z \to \ell\ell$ and $J/\psi \to \ell\ell$ events in bins of the probe lepton's p_{T} and η. The finite statistics of events in each (p_{T}, η)-bin and the differences with respect to simulation were used to define the corresponding uncertainties. It is worthwhile noting that with four leptons in the final state, single-lepton efficiency uncertainties could have as large as a four-fold effect on the final

event yields. The range of uncertainties on event rates was from 4% (4μ) to 10% ($4e$). The integrated luminosity uncertainty was less than 3%.

Systematic uncertainties on the "reducible" background yields, coming from the limited number of events in the control regions and from the imperfect knowledge of transfer factors, were in the $20-40\%$ range.

6.3.2. *Shape uncertainties*

For a low-mass Higgs boson ($m_H < 300$ GeV), the shape of the signal four-lepton mass distribution could be affected by uncertainties on the absolute electron/muon momentum scales and on the electron/muon momentum resolution. These uncertainties were particularly important in the measurements of the mass and width of the discovered boson and are described in detail in Sec. 8, where these measurements are presented.

For a high-mass Higgs boson ($m_H > 300$ GeV), the observable four-lepton mass distribution was defined by the intrinsic Higgs boson mass shape, which was subject to substantial theoretical uncertainties. In the earlier ATLAS and CMS searches, the narrow-width approximation encoded in POWHEG was used. To account for the poor description of the four-lepton mass lineshape for a heavy Higgs boson by the narrow-width approximation, a large ad hoc systematic uncertainty[23] on signal event yield, parametrised as $150\%\times(m_H/\text{TeV})^3$, was used. In the more recent analyses, POWHEG samples were reweighted by using the predictions for the mass lineshape calculated in the complex-pole scheme,[24] which also provided a more coherent treatment of the lineshape uncertainties.

Various sources of uncertainties on distribution shapes of other variables used in different analyses (e.g., four-lepton kinematic discriminants, VBF discriminants, etc.) were studied and found to have a negligible impact on the relevant results.

7. Observation of a new boson in the SM Higgs boson search

The SM Higgs boson was searched for in the mass range 110–1000 GeV. To quantify the search results, both ATLAS and CMS used the profile-likelihood-ratio test statistics, given by Eqs. (**??**) and (**??**) with unbinned likelihoods. A simplified view of the full likelihood is:

$$\mathcal{L}(\text{data}\,|\,b+\mu s) = \prod_k \mathcal{L}_k(\text{data}\,|\,b+\mu s)\,, \tag{5.3}$$

$$\text{with } \mathcal{L}_k(\text{data}\,|\,b+\mu s) = e^{-B_k-\mu S_k}\cdot\frac{(B_k+\mu S_k)^{N_k}}{N_k!}\cdot\prod_i \mathcal{F}_k(\mathcal{O}_i\,|\,b+\mu s)\,,$$

where the index k enumerates different event categories, each with N_k observed events and the total expected background events B_k and signal events μS_k. The factor μ is a signal strength modifier common for all event categories. Index i runs over all events in each category, and $\mathcal{F}_k(\mathcal{O}\,|\,b+\mu s)$ is the probability density function (pdf) of a set of observables $\mathcal{O}$ for an event in category k under the "$b+\mu s$" hypothesis, i.e. the nominal expected background plus the SM Higgs boson signal, whose event yields were scaled by the factor μ.

In the search for the Higgs boson, ATLAS used 8 categories (two centre-of-mass energies times four final-state flavours). The categorization by production mechanism was not used. As far as the observables $\mathcal{O}$ are concerned, the statistical analysis was performed in each of the 8 categories using 2D-*pdf*'s: $\mathcal{F}(m_{4\ell}, \text{BDT}_{\text{ZZ}^*})$. CMS used 12 event categories (two centre-of-mass energies, three final state flavours, two production tag categories) and 3D-*pdf*'s in each category: $\mathcal{F}(m_{4\ell}, D^{\text{kin}}_{\text{bkg}}, D_{jet})$ for dijet-tagged events; $\mathcal{F}(m_{4\ell}, D^{\text{kin}}_{\text{bkg}}, p^{4\ell}_{\text{T}})$ for untagged events.

In comparison to using four-lepton mass alone, adding the four-lepton kinematic discriminants against the ZZ background, BDT_{ZZ^*} (ATLAS) and $D^{\text{kin}}_{\text{bkg}}$ (CMS), helped increase the Higgs boson search sensitivity by as much as 20-30% in the explored range of possible Higgs boson masses.

Adding the dijet categorization in combination with using observables sensitive to vector-boson-fusion (VBF) Higgs boson production improved the search sensitivity by as much as 40% for a 1-TeV Higgs boson. However, in the low mass range, the VBF event yield relative to gluon fusion was expected to be very small and the gain in the search sensitivity from including these observables was less than 2% near $m_H \sim 125$ GeV. The dijet categorization, of course, was important for probing processes responsible for production of the discovered boson, as described in Sec. 9.

The number of events in simulation and control regions for "reducible" backgrounds were sufficient to populate 2D distributions and, hence, build 2D-pdfs, but too low to build statistically accurate 3D-pdfs. Hence, the 3D probability density functions used by CMS were constructed in a factorized form as a product of a 2D-pdf $\mathcal{F}(m_{4\ell}, D^{\text{kin}}_{\text{bkg}})$ and conditional 1D-pdf

$p(z\,|\,m_{4\ell})$, where z would stand for either D_{jet} or $p_{\mathrm{T}}^{4\ell}$. Using simulation, it was checked that neither D_{jet} nor $p_{\mathrm{T}}^{4\ell}$ correlated with the kinematic discriminant $D_{\mathrm{bkg}}^{\mathrm{kin}}$. This was expected since the kinematic discriminant depended on properties of four leptons in their centre-of-mass frame where there would be no information on jets or four-lepton system $p_{\mathrm{T}}^{4\ell}$ observed in the lab frame. The correlation, which might arise only from second-order acceptance effects, was found to be negligibly small.

Using the example of CMS results, Fig. 5.12 presents the 95% CL upper limits on the signal-strength modifier, $\mu = \sigma/\sigma_{\mathrm{SM}}$, as a function of m_H. In the mass range where $\mu < 1$ (114.5–119 and 129.5–832 GeV), the SM Higgs boson was excluded at 95% CL.

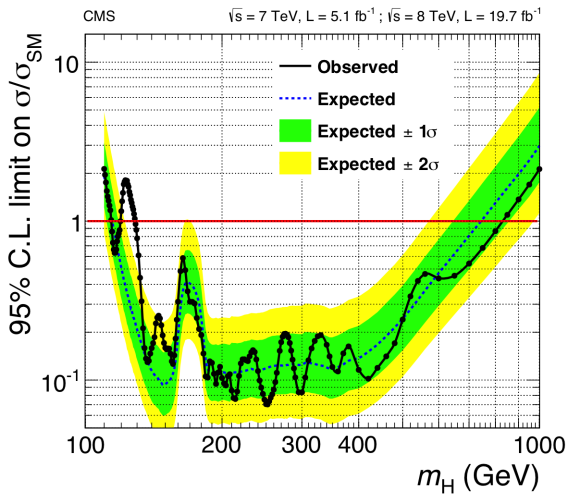

Fig. 5.12. Signal strength $\mu = \sigma_{\mathrm{H}}/\sigma_{\mathrm{H}}^{\mathrm{SM}}$ excluded by CMS experiments at 95% CL as a function of the hypothesised Higgs boson mass m_H.

The oscillations of the observed 95% CL upper limits around the median expected limits, assuming the background-only hypothesis, is a direct consequence of the high mass resolution, which results in observations for hypothesised Higgs bosons with nearby masses to be statistically independent. The sensitivity to a heavier SM Higgs boson is reduced owing to the the lower expected production rate in combination with the increasing natural width of the resonance. The steep loss of sensitivity at the lower end of the mass range is due to the diminishing branching fraction

$\mathcal{B}(H \to ZZ^*)$ channel and reduced reconstruction and selection efficiency for low-p_{T} leptons. For $2\,m_W < m_H < 2\,m_Z$, $\mathcal{B}(H \to ZZ^*)$ is very small, which propagates into a considerable loss of sensitivity in this mass range as well.

In most of the explored Higgs boson mass range, the observed limits were generally within the 68% or 95% bands around the median expected values and, hence, statistically compatible with the background-only hypothesis. However, in the range $119 < m_H < 129.5$ GeV, the limits were considerably weaker than expected in the absence of the SM Higgs boson. Despite having reached the SM Higgs boson sensitivity in this low-mass range, neither experiment could exclude the SM Higgs boson there, due to the excesses of events observed near 125 GeV.

To quantify the inconsistency of the observed excesses near 125 GeV with the background-only hypothesis, Fig. 5.13 shows a scan of the local p-value as a function of m_{H}, as obtained by ATLAS and CMS experiments. The probabilities for background fluctuating near that mass at least as high as observed were $\sim 10^{-14}$ (ATLAS) and 5×10^{-12} (CMS), which corresponded to statistical significances of $8.2\,\sigma$ and $6.8\,\sigma$, respectively. The very low probability for the excesses to arise from statistical fluctuations of background implied that both ATLAS and CMS observed a new boson[‖] with a mass near 125 GeV and decaying to four leptons.

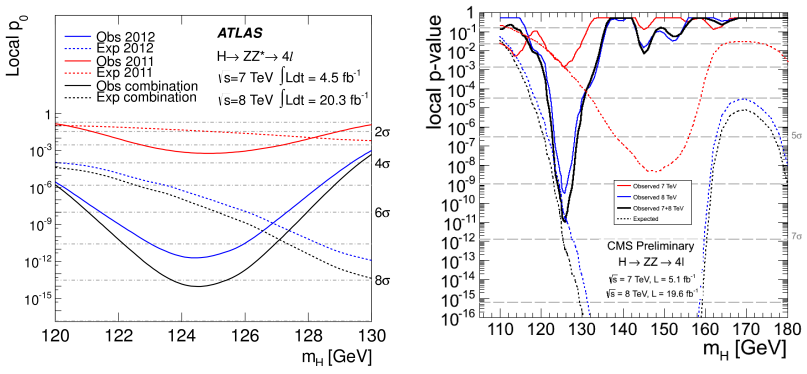

(a) (b)

Fig. 5.13. Local p-value p_0 for (a) ATLAS and (b) CMS searches for the SM Higg boson as a function of the hypothesised Higgs boson mass.

[‖] A particle decaying to even number of fermions must be a boson.

The dashed lines in Fig. 5.13 indicate the expected significances at different values of m_H, should the SM Higgs boson at those masses have existed. ATLAS observed an excess larger than expected for a SM Higgs boson with a mass near 125 GeV, while CMS observed an excess with about the expected significance. The statistical compatibility of the observed excesses with the expectations for the SM Higgs boson are discussed in Sec. 9.

Figure 5.14 shows an event display of a representative four-electron Higgs boson candidate. No other high momentum tracks or high energy deposits in calorimeters are seen next to the electrons, which implies that all four electrons in the event are isolated.

8. Mass and total width of the new boson

8.1. *Mass*

The mass of the observed boson was measured from a m_{H}-scan of the unbinned negative log-likelihood ratio, $-2\,\Delta \ln \mathcal{L}(\mathrm{data}\,|\,m_H)$. In this fit, the overall signal strength was allowed to float, while the relative event yields in the $4e$, 4μ, and $2e2\mu$ final states were assumed to be the same as for the SM Higgs boson.

With all nuisance parameters refit to maximise the likelihood at each m_H, the scan provided the total uncertainty of the measurement, as described in Appendix **??**. Statistical uncertainties on the measured masses were evaluated by performing the scan with all nuisance parameters, except for the overall signal strength, fixed at their best-fit values. The systematic uncertainty was evaluated as the difference in quadrature between the total and statistical uncertainties: $\sigma^2_{syst} = \sigma^2_{tot} - \sigma^2_{stat}$. The likelihood scans corresponding to the ATLAS, CMS, and combined ATLAS+CMS[12] data are shown in Fig. 5.15(a), while the numerical results obtained from these scans are presented in Table 5.5.

Table 5.5. Mass measurements for the observed boson by ATLAS, CMS, and ATLAS+CMS combination. The 95% CL limits on the intrinsic total width Γ_{tot} from the four-lepton resonance peak fit, as obtained by ATLAS and CMS, are also reported.

dataset used	measured mass	95% CL limit on Γ_{tot}
ATLAS	124.51 ± 0.52 (stat) ± 0.04 (syst) GeV	<2.6 GeV
CMS	125.59 ± 0.42 (stat) ± 0.17 (syst) GeV	<3.4 GeV
ATLAS+CMS	125.15 ± 0.37 (stat) ± 0.15 (syst) GeV	

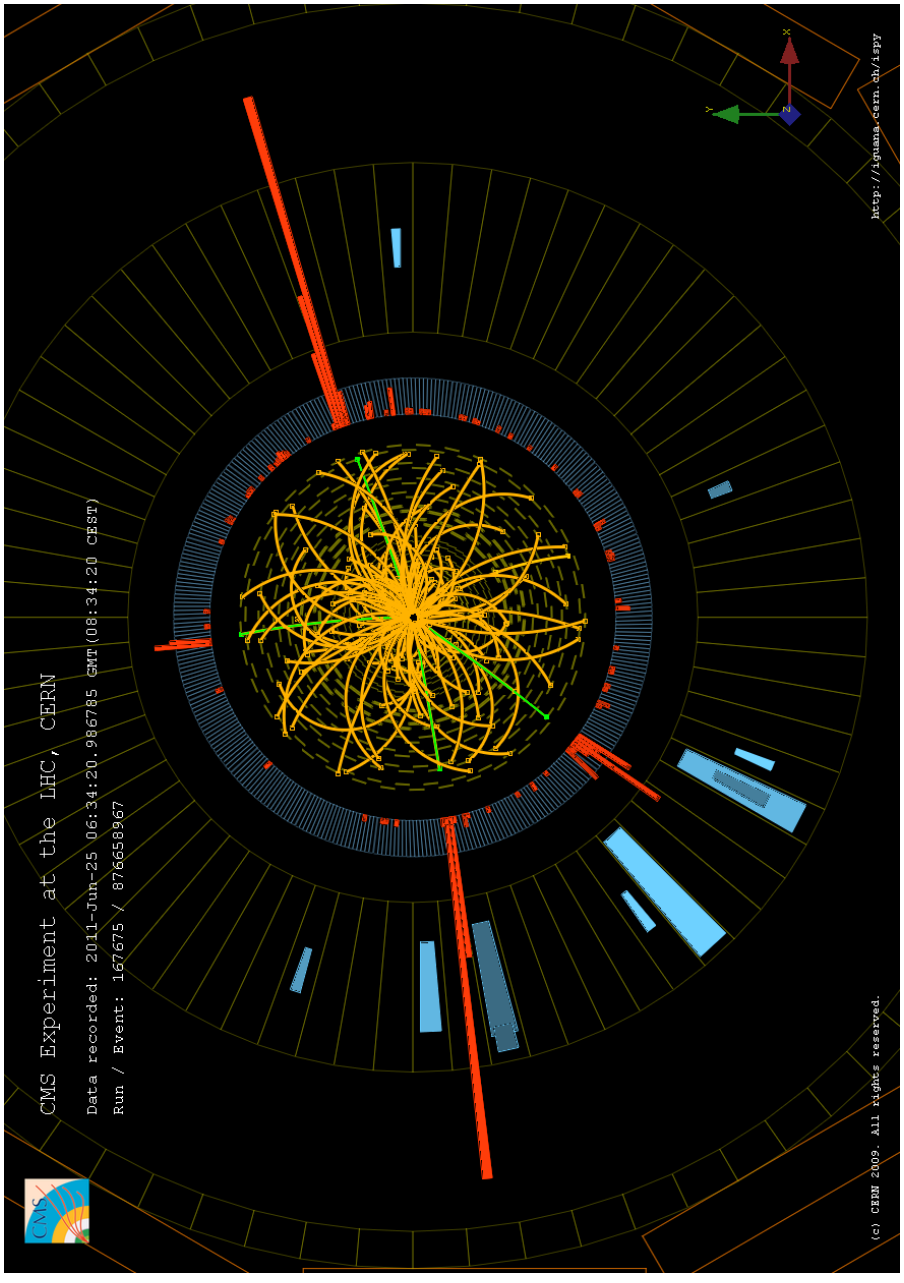

Fig. 5.14. Event display of a representative Higgs boson event candidate in the $H \to ZZ \to 4e$ decay mode observed by CMS. Tracks matched to the four pronounced electromagnetic clusters are highlighted in green. Invariant masses $m_{4\ell}$, m_{Z_1} and m_{Z_2} in this event are 125.7 GeV, 92.3 GeV and 27.2 GeV, respectively. All other tracks, highlighted in yellow, have a large curvature and correspond to low p_{T} charged particles. Amount of energy deposited in the hadron calorimeter (blue) is also small. No muon candidates are found in the event (muon detectors are outside of the figure box).

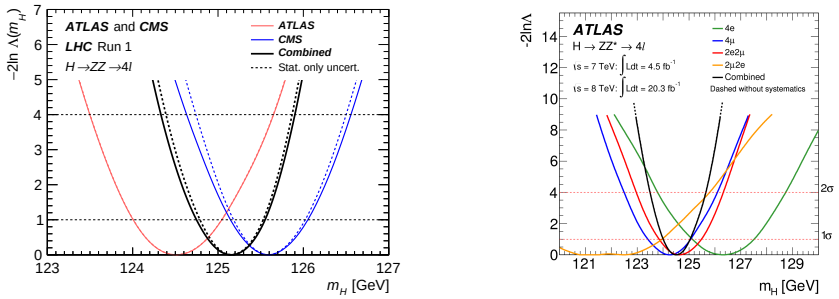

(a) (b)

Fig. 5.15. (a) Scan of the negative log-likelihood ratio as a function of the hypothesised mass of the new boson obtained for the ATLAS (red), CMS (blue), and combined ATLAS+CMS (black) data. The solid (dashed) lines correspond to scans with (without) systematic uncertainties. (b) Scan of the negative log-likelihood ratio for the different four-lepton final states as a function of the hypothesised mass of the new boson, as obtained by ATLAS.

ATLAS performed the measurement using two observables: the four-lepton invariant mass $m_{4\ell}$ and the kinematic discriminant BDT_{ZZ^*} (see Sec. 5), whose role in the mass fit was to give more weight to events that were more $H \to ZZ$ signal-like than $q\bar{q} \to ZZ$ background-like. Using of the kinematic discriminant in the fit helped improve the statistical uncertainty of the mass measurement by about 4%. Event categorizations based on the production-specific tags was not used in the mass measurements.

Even though events with four leptons of different flavours were treated as separate categories, individual events in the same final state could have different mass resolutions varying by as much as a factor of three, depending on leptons' p_T, η, and the overall reconstruction quality of leptons in a given event. Therefore, in addition to the four-lepton mass and kinematic discriminant, CMS added to the mass fit a third observable: an estimated per-event four-lepton mass uncertainty, $\sigma_{m_{4\ell}}$, whose purpose was to give more weight to events that had smaller uncertainties on the measured four-lepton mass. Including per-event four-lepton mass uncertainties improved the expected mass resolution by about 8%. It also allowed one to assign a more accurate uncertainty on the measured mass, given the four-lepton mass uncertainties for the observed events (instead of the expected average uncertainties). The latter was particularly important since the measurement was based on a small number of events. ATLAS used per-event four-

lepton uncertainties in a cross-check analysis of the main mass measurement result and in the direct measurements of the width of the discovered boson.

The main systematic uncertainties affecting the mass measurements were associated with the absolute electron/muon momentum scale calibration affecting the position of the peak, and on the electron/muon momentum resolution affecting the peak width. The scale of such potential biases could be evaluated by analysing the reconstructed peak position and width of Z, J/ψ, and Υ resonances for events sorted in bins of lepton's (p_{T}, η). In CMS, the differences in resonance mass peak positions between data and simulation in different data subsets was well covered by conservative envelopes of $\pm 0.1\%$ and $\pm 0.3\%$ uncertainties on the muon and electron momentum scales, respectively. ATLAS produced a more detailed map of uncertainties, as a function of lepton's p_{T} and η (e.g., see Fig. 5.16(a)). Using the detailed maps of uncertainties, the net systematic uncertainty on the mass measurement of the Higgs boson in $4e$ and 4μ final states was assessed to be of the order of $\pm 0.04\%$. The data-simulation differences in the widths of the Z, J/ψ, and Υ peaks were found to be well covered by assigning 20% uncertainties on the simulated muon/electron momentum measurement resolutions. The impact of this uncertainty on the mass measurement was negligible.

The ability to predict per-event mass resolutions was validated using $Z \to \ell\ell$ events, as shown in Fig. 5.16(b). It was found that a 20% uncertainty covers all observed differences between data and simulation. To use per-event four-lepton mass uncertainties, one had to extend the signal and background models to include appropriate $\mathcal{F}(\sigma_{m_{4\ell}} \,|\, m_{4\ell})$ *pdf*s. The $\mathcal{F}(\sigma_{m_{4\ell}} \,|\, m_{4\ell})$ distributions for Higgs boson and irreducible ZZ background were obtained from simulation and validated with data using $Z \to 4\ell$ events and $ZZ \to 4\ell$ events with $m_{4\ell} > 200$ GeV, where the "reducible" background contribution was negligible. For the "reducible" background, $\mathcal{F}(\sigma_{m_{4\ell}} \,|\, m_{4\ell})$ was obtained directly from data using events from the control region with two "tight" leptons and two "loose-but-not-tight" leptons (see Sec. 6).

Table 5.5 shows that the ATLAS and CMS mass measurements were compatible, which was a necessary prerequisite for the combination of the two results. The reason why CMS result was statistically more accurate, despite of a fewer number of observed events in the peak, was due to a somewhat better average four-lepton mass resolution (see Table 5.6) and due to using per-event four-lepton mass uncertainties. In dedicated studies preceding the combination, the dominant systematic uncertainties on lepton

momentum scales and resolutions were found to be uncorrelated between the two experiments.

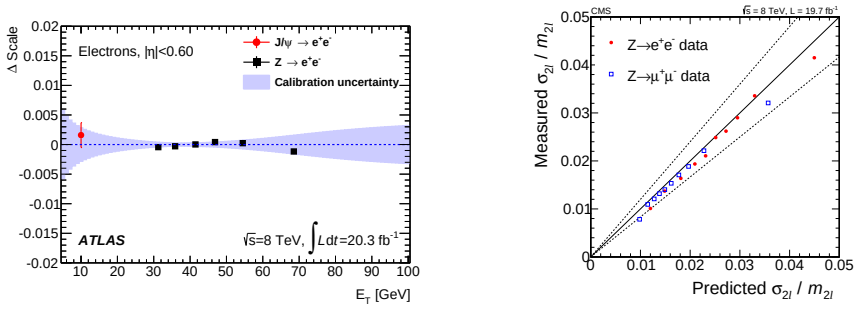

(a) (b)

Fig. 5.16. (a) Relative difference between the measured and the nominal electron energy scales, as a function of E_{T} for J/ψ and Z events in $|\eta| < 0.6$. The uncertainty on the nominal energy scale is shown by the shaded band. (b) Measured-versus-predicted relative dilepton mass resolution for $Z \to e^+e^-/\mu^+\mu^-$ events in data. The dashed lines represent the $\pm 20\%$ systematic uncertainty assigned to predictions of per-event mass resolutions.

8.2. *Total width*

The spread of events in the four-lepton mass peak serves as a direct, *model-independent*, probe of the total intrinsic width Γ_{tot} of the observed resonance. Although the expected sensitivity, $\delta\Gamma_{\mathrm{tot}} \sim \mathcal{O}(1)$ GeV, was by far larger than the expected SM Higgs boson width of 4.2 MeV, the measurement was important in the context of models beyond the standard model. For example, an observation of a non-zero width might imply the existence of more than one Higgs boson with a mass split comparable to the instrumental resolution. Both ATLAS and CMS observed that the excess near 125 GeV was consistent with the hypothesis of a single boson of a small total width. The obtained 95% CL upper bounds on the total width are shown in Table 5.5. Limits on the total width of the observed boson obtained in studies of the high-mass four-lepton events, where the observed boson was expected to contribute via its far off-shell production, are discussed in Sec. 12.

8.3. *Cross-checks*

By exploiting the independence of the electron and muon momentum scales one could perform a cross-check of the mass measurement results by comparing measurements in the different final states. Figure 5.15(b) shows the ATLAS mass likelihood scans for the four channels used in the analysis. The results obtained by ATLAS and CMS in different channels did not display any statistically significant biases.

In addition, the four-lepton mass peak near 91 GeV (see Fig. 5.8) arising from rare $Z \to 4\ell$ decays[29,30] (see Fig. 5.3(b)) could be used as a "standard candle" for a direct validation of the mass and width reconstruction of the newly discovered boson. The Z boson mass and width measured by CMS using $Z \to 4\ell$ events were 91.16 ± 0.23 GeV and $2.98^{+0.54}_{-0.50}$ GeV, respectively, in a good agreement with the world average values.[31] Note that the Z boson mass measurement uncertainty was lower than the uncertainty on the Higgs boson mass.

9. Signal strength

The signal strength modifier, μ, acts as a common scale factor on the number of events predicted by the SM for each Higgs boson signal process, or, equivalently, it scales the SM predicted cross section times branching fraction, $\sigma_{\rm SM} \cdot \mathcal{B}_{\rm SM}$. The signal strength values measured by ATLAS and CMS are shown in Table 5.6. The ATLAS and CMS results were statistically compatible with each other and with the expectations for the SM Higgs boson, i.e. with $\mu = 1$.

When comparing the obtained μ values, one needs to keep in mind the assumed Higgs boson masses at which they were evaluated. The *expected* signal event yield for the SM $H \to ZZ \to 4\ell$ channel increases at a rate of 7.2%/GeV as a function of the assumed Higgs boson mass near 125 GeV.

Table 5.6. Measurements of the overall (μ) as well as fermionic and bosonic ($\mu_{\rm F}$ and $\mu_{\rm V}$) signal strengths. The ATLAS result is evaluated at the ATLAS combined Higgs boson mass.[6] The CMS results are at the best-fit mass measured in the four-lepton channel alone.

	μ	$\mu_{\rm F}$	$\mu_{\rm V}$
ATLAS at $m_H = 125.4$ GeV	$1.44^{+0.34}_{-0.31}(\text{stat})^{+0.21}_{-0.11}(\text{syst})$	$1.7^{+0.5}_{-0.4}$	$0.3^{+1.6}_{-0.9}$
CMS at $m_H = 125.6$ GeV	$0.93^{+0.26}_{-0.23}(\text{stat})^{+0.13}_{-0.09}(\text{syst})$	$0.80^{+0.46}_{-0.36}$	$1.7^{+2.2}_{-2.1}$

These measurements were extended to probe signal strength factors for specific production modes. In this analysis, the production mechanisms were grouped into "fermionic" and "bosonic". The "fermionic" group consisted of the gluon-gluon fusion, $t\bar{t}H$, and $b\bar{b}H$ modes. The "bosonic" group comprised VBF, WH, and ZH production. Respective signal strength modifiers, μ_F and μ_V, were introduced to scale the expected SM Higgs boson event yields in each group and then fitted to the data in the production-tagged categories. The fit results are presented in Fig. 5.17. The best fit values for (μ_F, μ_V), shown in Table 5.6, were found to be consistent with the SM Higgs boson expectation, i.e. $(\mu_F, \mu_V) = (1, 1)$.

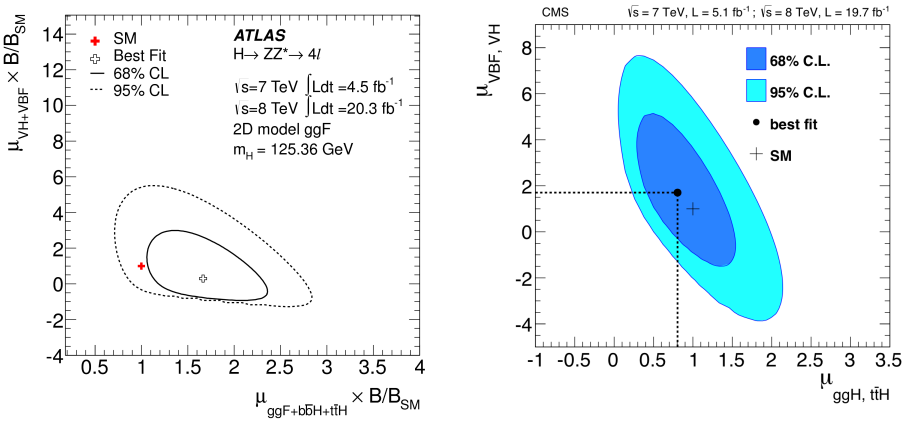

(a) ATLAS (b) CMS

Fig. 5.17. Simultaneous fit for signal strengths μ_F (x-axis) and μ_V (y-axis) by (a) ATLAS and (b) CMS. The best-fit values and the 68% (95%) CL contours are shown. The point (1,1), indicated by +, corresponds to the SM Higgs boson expectations.

Since the line $\mu_F = 0$ lies outside the 95% CL contour, the measurement established a non-zero fermionic coupling for the observed boson in the context of the tested two-parameter model. With the current amount of data, the $H \to ZZ \to 4\ell$ analysis did not yet reach sufficient sensitivity to establish explicitly the presence of VBF+VH production. As seen from Fig. 5.17, for $\mu_V = 0$ there was a range of μ_F values statistically compatible with the data.** However, the observed decays to the ZZ final state imply

**Technically, *pdf*s used in construction of unbinned likelihoods to describe the overall event probability density are checked to be positive definite, where data events are observed. This effectively limits the magnitude of possible negative values of μ_V for a given

a non-zero coupling of the discovered boson to Z bosons.

10. Fiducial total and differential cross sections

The extrapolation of event rates, measured within the detector acceptance, towards a total cross section can vary by a large factor, depending on the assumed production mechanism (e.g. by a factor of two for $gg \to H$ vs $q\bar{q} \to H$). Also, some signal selection efficiencies have a strong model-dependence (e.g. the lepton isolation efficiency is about 40% smaller for $gg \to ttH$ in comparison to $gg \to H$). To minimize model-dependence of the obtained results, measurements of inclusive and differential cross sections[32,33] were performed within a carefully selected fiducial volume, defined at the generator level, for which theoretical predictions could be made. The fiducial volume was closely matched to the four-lepton event selection criteria summarised in Table 5.1. ATLAS did not include the lepton isolation in the fiducial volume definition, while CMS did. Hence, ATLAS results are valid for models with jet activity similar to that expected for the SM Higgs boson production. CMS results do not have such a limitation.

The inclusive cross section for a resonance to produce four leptons at 8 TeV within the fiducial volume defined by ATLAS was measured to be $2.11^{+0.53}_{-0.47}(\text{stat}) \pm 0.08(\text{syst})$ fb, while the expected value for the SM Higgs boson was 1.30 ± 0.13 fb. The CMS results, obtained in the tighter fiducial volume, are shown in Fig. 5.18 (a). The measured fiducial cross section at 8 TeV was $1.11\ ^{+0.41}_{-0.35}(\text{stat})\ ^{+0.14}_{-0.10}(\text{syst})$ fb, with the expectation for the SM Higgs boson being 1.15 ± 0.13 fb.

The differential cross section measurements were performed in several production related observables, including: Higgs boson's transverse momentum and rapidity, associated jet multiplicity, transverse momentum of the leading jet, etc. Differential cross sections related to decay-related observables were also studied. As an example, Fig. 5.18 (b) shows the differential cross section measurements for the Higgs boson's transverse momentum, $p_{\mathrm{T},H}$. The results were found to be consistent with predictions, while the statistical precision of the measurements was not yet accurate enough to distinguish between different theoretical calculations for the SM Higgs boson.

μ_F and vice versa. The clipping of the ATLAS contours at the bottom was due to an event with a relatively high VBF-like purity.

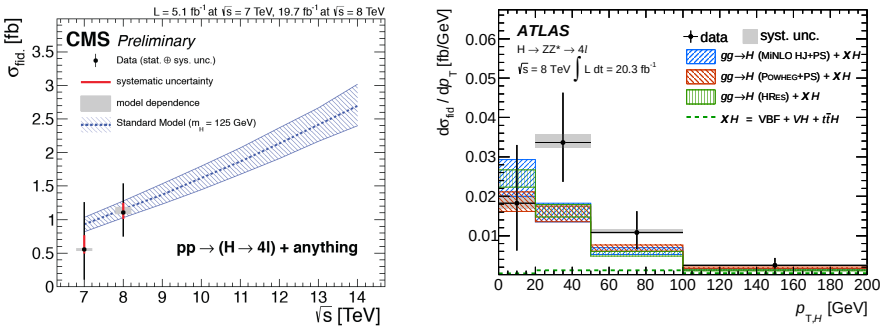

(a) (b)

Fig. 5.18. (a) Fiducial cross sections measured at 7 and 8 TeV and theoretical predictions in the 7–14 TeV range. (b) Differential fiducial cross section for the transverse momentum $p_{\mathrm{T},H}$ of the observed boson. Several theoretical calculations are presented, along with their uncertainties, as hatched blocks.

11. Determination of the spin-parity quantum numbers

After the discovery of the 125 GeV boson and establishing its mass and signal strength with respect to the expectations for the SM Higgs boson of that mass, it was important to test the compatibility of its spin-parity quantum numbers with those expected for the SM Higgs boson ($\mathrm{J^P} = 0^+$). The charge conjugation parity of the observed boson was set to $\mathrm{C} = +1$ by the observation of $\gamma\gamma$ decays, which also excluded $\mathrm{J} = 1$ by the Landau-Yang theorem, as described in Chapter **??**, Sec. **??**. A boson with generic spin-parity quantum numbers is henceforth denoted as X.

Before presenting the spin-parity analyses carried out with the four-lepton final state, a brief phenomenological preamble is given in Sec. 11.1. It is followed by Sec. 11.2 describing results of pair-wise tests of data compatibility with the SM Higgs boson versus various alternative (exotic) boson models. Analyses aiming to detect admixtures of anomalous non-SM like amplitudes in the four-lepton decays of the observed boson are described in Sec. 11.3. The presented results are based on Refs. [4,5,9,13].

11.1. *Phenomenological considerations*

The $X \to ZZ \to 4\ell$ and $X \to WW \to 2\ell 2\nu$ four-body decay modes are well suited for probing all possible $\mathrm{J^P}$ spin-parity states, albeit with different levels of sensitivities. The diphoton decays cannot be used for probing

alternative J = 0 amplitudes. Two photons emerging from a spin-zero state decays are back-to-back in the boson's rest frame, with the diphoton axis direction uniformly distributed in stereo angle, and, unless one can measure the two photons' polarisations, provide no handles for studying the different possible decay amplitudes that can be associated with a J = 0 state. For a boson with J = 2, distribution of the diphoton axis direction with respect to the beam line, however, is not uniform and depends on the underlying structures in both production and decay amplitudes.

11.1.1. *Spin zero*

The Effective Field Theory (EFT) Lagrangian up to dimension-five operators for a spin-zero state decaying to two vector bosons, $X \to VV$, is given by Eq. (**??**) in Chapter **??**, Sec. **??**. The first dimension-three operator corresponds to the SM Higgs boson. The other three α-, β-, γ-terms are dimension-five operators and can be thought of as effective operators for loop-induced decays. In this convention the "effective couplings" α, β, γ absorb actual couplings, mass scales of particles in the loops (relative to the vacuum expectation value of the Higgs field), loop factors, etc. The α- and β-terms are even-parity scalars, kinematically distinguishable from the SM Higgs boson, while the γ-term corresponds to a pseudo-scalar. In fact, SM particles contribute to all three terms, but at a very small level:[15,34] $\alpha \sim \beta \sim \mathcal{O}(\alpha_{\rm EW}) \sim 10^{-2}$ and $\gamma \sim \mathcal{O}(10^{-11})$. In SM, it takes at least three loops to generate a pseudoscalar-like term.

11.1.2. *Spin one*

The spin-one hypothesis was studied using $X \to ZZ$ and/or $X \to WW$ decays. One can consider those studies either as a test carried out independently of the observation of di-photon decays, prohibiting spin-one states, or as a test for a possible conspiracy of multiple nearly mass-degenerate states with different quantum numbers. In the case of the spin-one resonance, there are two distinct decay amplitudes corresponding to a vector (1^-) and a pseudo-vector (1^+),[35] both of which correspond to dim-four operators. Note that production of spin-one state via gluon fusion must be strongly suppressed; for on-shell gluons, production amplitude $\mathcal{A}(gg \to X)$ must be zero by the very same Landau-Yang theorem that forbids decays to diphoton final states.

11.1.3. *Spin two*

As mentioned in Chapter **??**, there is not a self-consistent quantum field theory of elementary spin-two massive states. Moreover, within the EFT framework, one can write out a large number of XVV and Xff Lagrangian terms, associated with kinematically distinguishable spin-two states. All this ensures complications for experimental analyses aiming to assess the relative odds of the observed boson being an exotic—perhaps, composite—spin-two state or a SM-like Higgs boson.

For a colour-, weak- and electromagnetic-singlet spin-two resonance (henceforth denoted as 2^+_m, following notations introduced in Ref. [15]), the Lagrangian is unique:[36]

$$\mathcal{L} \sim -\frac{1}{\Lambda}\sum_i \kappa_i T^i_{\mu\nu} X^{\mu\nu}, \tag{5.4}$$

where i runs over all SM particles and $T^i_{\mu\nu}$ is the energy-momentum tensor of particle i. This Lagrangian can be associated with the RS graviton,[37] in which case couplings κ_i to all SM particles are universal. However, the premise of universal couplings is obviously in a strong contradiction with the observed relative decay rates of the discovered boson (see Chapter **??**).

Therefore, one is compelled to consider a 2^+_m state with non-universal couplings. This, however, creates new problems. First, distributions of the production-related observables would strongly depend on the assumed relative couplings of X to quarks and gluons (assuming that the dominant production mechanism is $q\bar{q}/gg \rightarrow X$). Second, should the quark and gluon couplings be different, the X boson would acquire unitarity-violating behaviour manifesting itself in substantial X-boson's p_{T}-boosts at NLO.[36]

On the other hand, one can assume that the unitarity problems are resolved by yet-to-be-discovered new physics at higher energy scales and use the abnormal $p_T(X)$ distributions as yet another observable discriminating between 2^+_m and the SM Higgs boson for the case when $\kappa_q \neq \kappa_g$. The observed $p_{\mathrm{T}}(X)$ distributions in the $\gamma\gamma$ and ZZ decay modes (Sec. **??** in Chapter **??**, and Sec. 10 in this chapter, respectively), constrain the allowed range of non-universality to $0 \leq \kappa_q \lesssim 2\kappa_g$, see Ref. [13]. Finally, one should beware that, if a spin-two boson is produced in association with jets, its production-related observables are considerably modified with respect to those at LO (the effect does not exist for J = 0 and is expected to be negligible for J = 1 bosons).[36]

As stated at the beginning of this sub-section, from the EFT stand point, one can write many more Lagrangian terms associated with XVV

vertex. Ref. [15] defines 10 such terms, going up to dimension seven. In this context, the 2^+_m state is a combination of two out of these terms, the lowest dimension of which is denoted as 2^+_b. Notations for the alternative eight possibilities, consisting of dimension-five and dimension-seven operators, are: 2^+_h, 2^-_h, 2^+_{h2}, 2^+_{h3}, 2^+_{h6}, 2^+_{h7}, 2^-_{h9}, 2^-_{h10},.[9]

11.2. *Pair-wise tests: SM Higgs vs. alternative* $\mathbf{J^P}$ *states*

To test alternative J^P signal (X) hypotheses against the SM Higgs boson (H), both ATLAS and CMS opted for matrix-element discriminants. Cross checks using multivariate-observables trained using Boosted Decision Trees were also performed. The event categorizations by production mechanism were not used.

Probability density functions for an event to come from a given process could be written as follows:

$$\mathcal{F}(\mathcal{P}\,|\,\text{process}) \sim |\mathcal{A}_{\text{process}}(\mathcal{P})|^2 \cdot \epsilon(\mathcal{P}) \cdot \mathcal{F}(m_{4\ell}|\text{process})\,. \tag{5.5}$$

In this equation, $\mathcal{P}$ stands for momenta of four leptons in the final state, $\mathcal{A}_{\text{process}}(\mathcal{P})$ is the LO matrix elements calculated in the same manner as described in Sec. 5.2, $\epsilon(\mathcal{P})$ is the four-lepton reconstruction efficiency, $\mathcal{F}(m_{4\ell}|\text{process})$ is the four-lepton mass probability distribution function.[††]

With three main processes relevant to this analysis (SM Higgs boson H, exotic boson X, and background dominated by $q\bar{q} \to ZZ$), there were only two independent ratios that could be formed; the two actually used were:

$$d_{\text{X}} = \frac{\mathcal{F}(\mathcal{P}\,|\,\text{X})}{\mathcal{F}(\mathcal{P}\,|\,\text{H})} = \frac{|\mathcal{A}_{\text{X}}|^2}{|\mathcal{A}_{\text{H}}|^2}\,, \tag{5.6}$$

$$d_{\text{bkg}} = \frac{\mathcal{F}(\mathcal{P}\,|\,\text{bkg})}{\mathcal{F}(\mathcal{P}\,|\,\text{H})} = \frac{|\mathcal{A}_{\text{ZZ}}|^2}{|\mathcal{A}_{\text{H}}|^2} \cdot \frac{\mathcal{F}(m_{4\ell}|\text{bkg})}{\mathcal{F}(m_{4\ell}|H)}\,. \tag{5.7}$$

The first one separated the alternative signal hypothesis from the SM Higgs boson, while the second discriminated against backgrounds. In these ratios the lepton reconstruction efficiencies, to a good approximation, cancel out. For convenience, the discriminants were monotonically transformed to be constrained between 0 and 1, and the analyses were performed by building likelihoods of the observed events in the space of the two transformed observables, D_{X} and D_{bkg}.

By using the 2D probability density functions $pdf(D_{\text{bkg}}, D_{\text{X}})$ and taking into account the expected event yields for backgrounds, the observed test

[††]ATLAS used events only in a narrow mass-window around the peak and did not include $\mathcal{F}(m_{4\ell}|\text{process})$ in their spin-parity studies.

statistic values were calculated as follows:

$$q = -2 \ln \frac{\mathcal{L}_{max}(\text{ data} \,|\, \hat{\mu}_X \cdot X + \text{bkg}, \hat{\theta}_X)}{\mathcal{L}_{max}(\text{ data} \,|\, \hat{\mu}_H \cdot H + \text{bkg}, \hat{\theta}_H)} \,. \tag{5.8}$$

The H and X signal event yields were not constrained by any external assumptions and treated on par with all other nuisance parameters (θ) in the fits maximizing the likelihoods in the numerator and denominator.

The observed value of test statistic, q^{obs}, were compared to the expectations obtained by simulating pseudo-observations generated using the same *pdf*s. Numbers of signal events in pseudo-experiments were drawn from the Poisson distributions with the best-fit rates as obtained in the data. Figure 5.19 shows ATLAS and CMS results of testing the pseudoscalar against the SM Higgs boson hypotheses. The expected tests statistic distributions for the two hypotheses were well separated, indicating that both experiments had reached fair sensitivities to distinguish between pure 0^- and SM-like Higgs boson states. The observed test statistic values were in the core of the distributions expected for the SM Higgs boson (and, hence, consistent with the SM Higgs boson hypothesis) and were far in the tails of the distributions expected for a pure pseudoscalar, thus strongly disfavouring this hypothesis.

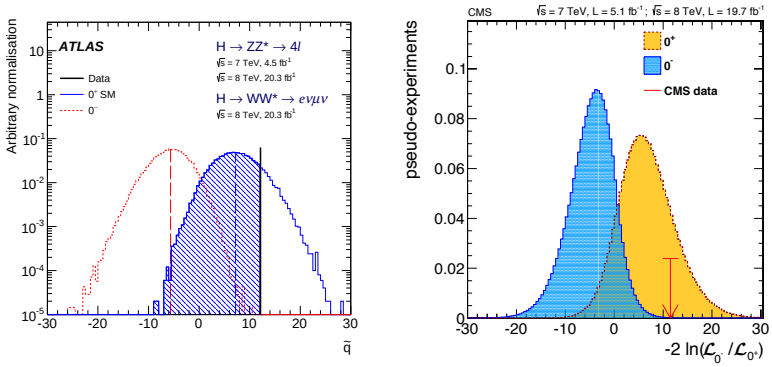

(a) (b)

Fig. 5.19. Test statistic distributions for the SM Higgs boson and the pseudo-scalar hypotheses for (a) ATLAS and (b) CMS. The observed values of the test statistic are also shown.

Quantitatively, deviations of q^{obs} from the expected medians were characterized by p-values, converted then into a number of standard deviations.

On the example of ATLAS, the deviation of observed $q^{\rm obs}$ from the median-expected for the SM Higgs boson had a p-value of 88% (area of the blue histogram on the left side from the observation), which would correspond to -1.2 standard deviations ($\Delta_q = -1.2\sigma$). Following the statistical convention, deviations Δ_q from medians away from an alternative hypothesis distribution were counted as negative. The p-value for the pseudoscalar hypothesis (area of the red histogram on the right side from the observation) comprised 1.2×10^{-5}, corresponding to $\Delta_q = +4.2\sigma$. The $\mathrm{CL_s}$ values for ATLAS and CMS were 0.01% and 0.05%, respectively, which implied that the hypothesis of a psedoscalar was excluded by each experiment with more than 99.9% CL. ATLAS and CMS limits were somewhat tighter than expected due to the "lucky" statistical fluctuations of data in both experiments: the observed value of the test statistic was on the right from the median value expected for the SM Higgs boson, which made the observations particularly unlikely for a pseudoscalar.

Table 5.7 shows the ATLAS and CMS results of all alternative $\mathrm{J^P}$ states tested by both collaborations. CMS also tested nine other, more exotic, amplitude tensor structures for spin-two boson decays $X \to VV$, corresponding to higher-dimension operators (2^+_b, 2^+_h, 2^-_h, 2^+_{h2}, 2^+_{h3}, 2^+_{h6}, 2^+_{h7}, 2^-_{h9}, 2^-_{h10}). All tested exotic boson models were excluded at 99% CL or higher, while the data agreed well with the SM Higgs boson in each of the nine tests.

Table 5.7. Results of testing alternative $\mathrm{J^P}$ state hypotheses against the SM Higgs boson (H). See text for explanations.

$\mathrm{J^P}$		ATLAS			CMS (any production)		
	$xx \to X$	$\Delta_q(\mathrm{H})$	$\Delta_q(\mathrm{J^P})$	$\mathrm{CL_s}$	$\Delta_q(\mathrm{H})$	$\Delta_q(\mathrm{J^P})$	$\mathrm{CL_s}$
0^-		-1.2σ	$+4.2\sigma$	0.01%	-1.0σ	$+3.8\sigma$	0.05%
0^+_h		-0.8σ	$+3.4\sigma$	0.18%	-0.3σ	$+2.1\sigma$	4.5%
1^-	$q\bar{q} \to 1^-$	$+1.0\sigma$	$+1.6\sigma$	6.0%	-2.0σ	$> 5.0\sigma$	<0.001%
1^+	$q\bar{q} \to 1^+$	-0.1σ	$+3.1\sigma$	0.2%	-2.3σ	$> 5.0\sigma$	<0.001%
2^+_m	$(q\bar{q}, gg) \to 2^+_m$	-0.4σ	$+2.7\sigma$	0.97%	-1.6σ	$+3.4\sigma$	0.71%

Note that spin-zero hypothesis tests are not sensitive to the mechanism responsible for production of the observed boson, as a spin-zero state has no information on its production history in its center of mass frame. For other spins, kinematical properties of decay products are not completely

decoupled from the particles participating in the production.

ATLAS analyses assumed specific production mechanisms in their spin-one and spin-two tests. A spin-one particle cannot be produced via fusion of on-shell gluons (see Sec. 11.1); hence, the spin-one tests were performed assuming quark-antiquark annihilation. For the spin-two case, ATLAS probed various mixtures of quark-antiquark annihilation and gluon-gluon fusion; the most conservative limit among all of the tested mixtures is shown in the table.

CMS made their analyses nearly independent of an assumed production mechanism by integrating matrix elements for $xx \to X \to 4\ell$ over degrees of freedom connecting final state leptons and particles participating in production of X. This is equivalent to using $1 \to 4$ matrix elements $\mathcal{A}(X \to 4\ell)$ instead of $2 \to 1 \to 4$ matrix elements $\mathcal{A}(xx \to X \to 4\ell)$. The loss of sensitivity from such a generalization was typically less than 10%.

11.3. *Search for presence of anomalous decay amplitudes*

In addition to excluding hypotheses of pure non-SM like states, ATLAS and CMS probed the phenomenological possibility of a SM-like Higgs boson being mixed with α-, β-, and γ-terms in the spin-zero Lagrangian, given by Eq. (**??**). Testing for an admixture of a pseudoscalar (γ-term) was and will remain of a particular interest: should it be observed, it would open one more portal for CP-violating processes.

The analysis was performed in a variety of technical ways (all giving compatible results), one of which was identical to what was described above, with the only difference that in the discriminant given by Eq. (5.6), X would stand for a mixed state. Since absolute cross sections were not used in the discrimination (as in the case of pure states), the only relevant variables in these analyses were ratios of couplings. Table 5.8 summarizes the allowed 95% CL intervals for alternative spin-zero state admixtures.

Table 5.8. Obtained 95% CL intervals on the *allowed* couplings of alternative, not SM-like, spin-zero states with respect to those of the SM scalar state.

	α/κ	β/κ	γ/κ
ATLAS	not tested	$[-2.45, 0.75]$	$[-0.95, 2.85]$
CMS	$[-1.2, 1.5]$	$[-\infty, 0.69]$ $[1.9, 2.3]$	$[-2.2, 2.1]$

12. Total width determination via off-shell production

The total width for a SM Higgs boson with 125 GeV mass, $\Gamma_{\rm SM} = 4.2$ MeV, is approximately three orders of magnitude below the sensitivity of the direct measurements described in Sec. 8. As discussed in Chapter **??**, the yield and properties of high-mass ZZ events are sensitive to the width of the 125-GeV boson, with an important caveat that the actual numerical relationship is model-dependent. Following these considerations, both ATLAS and CMS pursued studies of high-mass ZZ events.[10,11] Events with $m_{4\ell} > 220$ GeV were used in both analyses. In this section, X refers to a resonance of 125 GeV with spin-parity quantum numbers identical to the SM Higgs boson and total width $\Gamma \neq \Gamma_{\rm SM}$.

To improve the measurement sensitivity, ATLAS and CMS introduced ME-based discriminants. With multiple distinct underlying physics processes involved ($q\bar{q} \to ZZ$ (Fig. 5.3(a)), $gg \to$ "box" $\to ZZ$ (Fig. 5.3(c)), $gg \to H \to ZZ$, $gg \to X \to ZZ$, and the signal-background interference between $gg \to$ "box" $\to ZZ$ and $gg \to H/X \to ZZ$, it was not surprising that discriminant implementations chosen by the two experiments were somewhat different.

CMS used the following discriminant:

$$d_{gg} = \frac{|\mathcal{A}(gg \to (\, X_{10}/\text{“box”}\,) \to ZZ)|^2}{|\mathcal{A}(q\bar{q} \to ZZ)|^2}, \tag{5.9}$$

Here, X_{10} denotes a boson with width $\Gamma_{10} = 10\,\Gamma_{SM}$. The factor of 10 was picked based on the expected experimental sensitivity to the width with the Run 1 data set. By construction, this discriminant helped separate the gg-induced processes from the $q\bar{q} \to ZZ$ background. Moreover, its shape was also sensitive to the boson's width Γ, as can be seen in Fig. 5.20 (a). For models with an X boson of a different width, this discriminant was somewhat sub-optimal. To get the maximum sensitivity, CMS performed its analysis in a 2D plane of two observables: four-lepton mass and the ME-based discriminant.

ATLAS defined its discriminant as follows:

$$d = \frac{|\mathcal{A}(gg \to H \to ZZ)|^2}{|\mathcal{A}(gg \to (\, H/\text{“box”}\,) \to ZZ)|^2 + c \cdot |\mathcal{A}(q\bar{q} \to ZZ)|^2}, \tag{5.10}$$

where c is an empirical constant, chosen to be 0.1, to approximately balance the two contributions in the denominator. The analysis was performed using the ME discriminant alone with a simple cut on four-lepton mass $m_{4\ell} > 220$ GeV. As seen from Fig. 5.20 (b), in addition to the overall

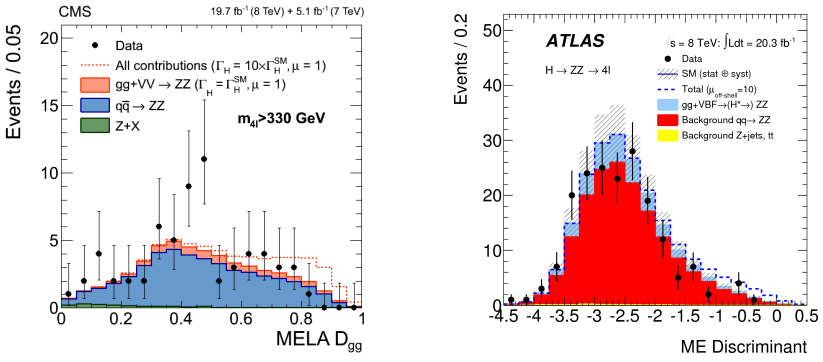

(a) CMS (b) ATLAS

Fig. 5.20. Distributions of events for matrix-element based observables used by (a) CMS and (b) ATLAS in the analyses probing the amount of off-shell Higgs boson production. The observables shown are monotonic transformations of the primary discriminants given by Eqs. (5.9) and (5.10). The CMS and ATLAS distributions are shown for $m_{4\ell} > 330$ and >220 GeV, respectively.

event yield, the distribution of the ATLAS ME-discriminant had a clear sensitivity to the width of the underlying boson.

The CMS scan of likelihood $\mathcal{L}(data\,|\,\Gamma)$, shown in Fig. 5.21(a), reveals that the best-fit width was close to zero and the upper bound on the total width could be set at $8.0 \times \Gamma_{\rm SM}$, or 33 MeV, at 95% CL. When the $H \to ZZ \to 4\ell$ analysis was combined with an analysis assessing the off-shell signal event rate in the $ZZ \to 2\ell 2\nu$ channel,[11] the limit at 95% CL on the width of the discovered boson became $5.4 \times \Gamma_{\rm SM}$, or 22 MeV.

Figure 5.21(b) shows the expected and observed results obtained by ATLAS in the 4ℓ analysis for the off-shell signal strength, $\mu_{\rm off-shell}$, a parameter defined as the ratio of the number of off-shell signal events to the number expected for the SM Higgs boson. Interference with $gg \to$ "box" $\to ZZ$ plays no role in the definition of $\mu_{\rm off-shell}$. The figure explicitly shows that the inferred limit on $\mu_{\rm off-shell}$ has a non-negligible dependence on the assumed K-factor for $gg \to$ "box" $\to ZZ$ background, expressed in units of the K-factor for $gg \to H^*$: $R^B_{H^*} = K(gg \to \text{"box"} \to ZZ)\,/\,K(gg \to H^*)$.[‡‡] To reinterpret the obtained results in the context of the observed boson's width, limits on $\mu_{\rm off-shell}$ need to be combined with measurements of the on-shell signal strength $\mu_{\rm on-shell}$. ATLAS did this exercise in the combi-

[‡‡]The CMS results were obtained in assumption of $R^B_{H^*} = 1$ with a 10% systematic uncertainty.

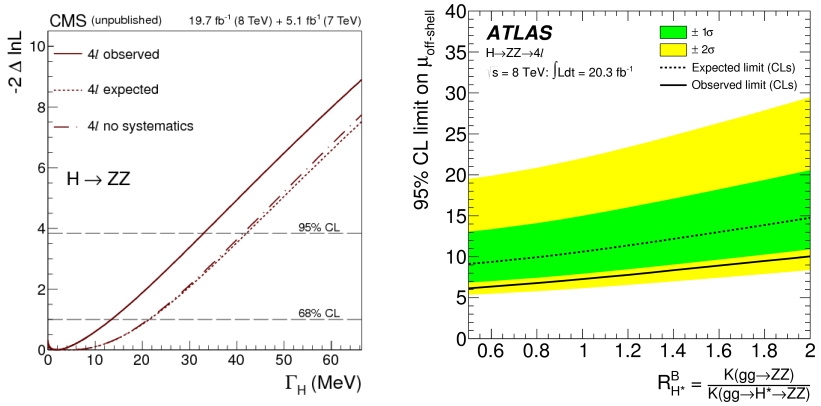

(a) (b)

Fig. 5.21. (a) Likelihood scan as a function of the total width of the observed boson from CMS. The solid line correspond to the observation, the dashed line to the expectation, while the dash-dotted line is the expectation neglecting systematic uncertainties. (b) The observed and expected 95% CL_s upper limits on the off-shell signal strength, $\mu_{\mathrm{off-shell}}$, as a function of R^B_{H*} (see text) from ATLAS.

nation of the $H \to ZZ \to 4\ell$, $ZZ \to 2\ell 2\nu$, and $WW \to e\nu\mu\nu$ analyses.[11] Assuming $R^B_{H*} = 1$, the obtained 95% CL limit was $\Gamma < 5.5 \times \Gamma_{\mathrm{SM}}$, or 23 MeV.

13. Summary and outlook

The ATLAS and CMS experiments searched for a Standard Model Higgs boson with a mass in the range 110–1000 GeV and decaying to the $ZZ \to 4\ell$ final state. Both experiments observed a narrow four-lepton resonance with a mass near 125 GeV with local statistical significances of 8.2σ and 6.8σ, respectively. This unambiguously established the existence of a new boson decaying to four leptons. The mass of the discovered boson was measured to be 124.5 ± 0.5 GeV (ATLAS), 125.6 ± 0.5 GeV (CMS), giving a combined mass measurement of 125.15 ± 0.37 (stat) ± 0.15 (syst) GeV. The best-fit signal signal strengths with respect to the expected event yield for the SM Higgs boson were $1.44^{+0.40}_{-0.33}$ (ATLAS) and $0.93^{+0.29}_{-0.25}$ (CMS). The Run 1 dataset was not yet sufficient to establish the presence of sub-leading production mechanisms such as VBF, VH, and $t\bar{t}H$. Inclusive differential distributions for a number of observables, such as transverse momentum and rapidity of the discovered boson, number of jets produced in association

with the boson and leading jet E_{T}, were found to be consistent with those expected for the SM Higgs boson, albeit with limited statistical accuracy. The angular distributions of leptons were statistically consistent with the new boson having spin-parity quantum numbers $\mathrm{J^P} = 0^+$, as expected for the SM Higgs boson, and were inconsistent at 95% CL or higher with alternative $\mathrm{J^P}$ hypotheses, which included pseudo-scalar, vector, pseudo-vector, and ten distinct spin-two tensor hypotheses. By comparing the on-shell event yield in the four-lepton final state to the ZZ and WW event rates at high masses, where the new boson would contribute via off-shell production, ATLAS and CMS set model-dependent upper limits on the total Breit-Wigner width of the resonance at 23 and 22 MeV at 95% CL . Within the experimental uncertainties, the ATLAS and CMS measurements were compatible with each other and, also, consistent with the expectations for the SM Higgs boson.

Over the next two decades, LHC is expected to deliver about 3000 fb^{-1} at a centre-of-mass energy near 14 TeV. The production cross section for the 125 GeV Standard Model Higgs boson at $\sqrt{s} = 14$ TeV increases by a factor of 2.6 with respect to 8 TeV. Therefore, the ultimate Higgs boson dataset will be about 300 times larger than the Run 1 dataset, which will allow for much more precise measurements than those described in this chapter and, also, provide opportunities for conducting completely new searches and measurements. The statistical uncertainty on the mass measurement will decrease to $(0.4\ \mathrm{GeV})/\sqrt{300} \sim 25$ MeV, or 0.02%. Reducing the corresponding systematic uncertainties to levels much lower than 0.02% will be challenging. Fiducial cross sections $\sigma(pp \to H \to ZZ \to 4\ell)$ can potentially be measured with about $(30\%)/\sqrt{300} \sim 2\%$ statistical precision, challenging the accuracy of theoretical predictions, while differential measurements will provide a wealth of information on the dynamics associated with the Higgs boson production. All main Higgs boson production modes should become detectable and the prevailing ones will be studied in detail. With such a large dataset, the expected 2σ-sensitivity of a search for an admixture of a CP-odd component in the HZZ coupling is estimated to be about $\gamma/\kappa \sim 0.5$[17] and ~ 0.25.[38] The decay mode $H \to \gamma^*\gamma^* \to 4\ell$ is expected to be observed and will allow one to probe the tensor structure of the H$\gamma\gamma$ coupling as well.[39] Studies assessing the ultimate precision of off-shell production measurements at LHC and the associated inference of the total Higgs boson width are under way. And, of course, searches for exotic 4ℓ decays of the 125 GeV Higgs boson (e.g. $H \to ZZ_{dark} \to 4\ell$[40]) and for additional heavier or lighter bosons decaying to the 4ℓ final state[41,42] will

continue and, one may hope, bear fruit.

References

1. ATLAS Collaboration, Observation of a new particle in the search for the Standard Model Higgs boson with the ATLAS detector at the LHC, *Phys. Lett.* **B716**, 1–29 (2012). doi: 10.1016/j.physletb.2012.08.020.
2. CMS Collaboration, Observation of a new boson at a mass of 125 GeV with the CMS experiment at the LHC, *Phys. Lett.* **B716**, 30–61 (2012). doi: 10.1016/j.physletb.2012.08.021.
3. LHC Higgs Cross Section Working Group, Handbook of LHC Higgs Cross Sections: 1. Inclusive Observables (2011). doi: 10.5170/CERN-2011-002. URL `http://arxiv.org/abs/1101.0593`.
4. CMS Collaboration, Measurement of the properties of a Higgs boson in the four-lepton final state, *Phys.Rev.* **D89**, 092007 (2014). doi: 10.1103/PhysRevD.89.092007.
5. ATLAS Collaboration, Evidence for the spin-0 nature of the Higgs boson using ATLAS data, *Phys.Lett.* **B726**, 120–144 (2013). doi: 10.1016/j.physletb.2013.08.026.
6. ATLAS Collaboration, Measurement of the Higgs boson mass from the $H \to \gamma\gamma$ and $H \to ZZ^* \to 4\ell$ channels with the ATLAS detector using 25 fb^{-1} of pp collision data, *Phys.Rev.* **D90**, 052004 (2014). doi: 10.1103/PhysRevD.90.052004.
7. ATLAS Collaboration, Measurements of Higgs boson production and couplings in the four-lepton channel in pp collisions at center-of-mass energies of 7 and 8 TeV with the ATLAS detector, *Phys.Rev.* **D91**(1), 012006 (2015). doi: 10.1103/PhysRevD.91.012006.
8. ATLAS Collaboration, Measurement of the muon reconstruction performance of the ATLAS detector using 2011 and 2012 LHC proton-proton collision data, *Eur.Phys.J.* **C74**(11), 3130 (2014). doi: 10.1140/epjc/s10052-014-3130-x.
9. CMS Collaboration, Constraints on the spin-parity and anomalous HVV couplings of the Higgs boson in proton collisions at 7 and 8 TeV, *Phys. Rev.* **D92** (1), 012004 (2015). doi: 10.1103/PhysRevD.92.012004.
10. CMS Collaboration, Constraints on the Higgs boson width from off-shell production and decay to Z-boson pairs, *Phys.Lett.* **B736**, 64 (2014). doi: 10.1016/j.physletb.2014.06.077.
11. ATLAS Collaboration, Constraints on the off-shell Higgs boson signal strength in the high-mass ZZ and WW final states with the ATLAS detector, *Eur. Phys. J.* **C75**(7), 335 (2015). doi: 10.1140/epjc/s10052-015-3542-2.
12. ATLAS and CMS Collaborations, Combined Measurement of the Higgs Boson Mass in pp Collisions at $\sqrt{s} = 7$ and 8 TeV with the ATLAS and CMS Experiments, *Phys.Rev.Lett.* **114**, 191803 (2015). doi: 10.1103/PhysRevLett.114.191803.

13. ATLAS Collaboration, Study of the spin and parity of the Higgs boson in diboson decays with the ATLAS detector, *Eur. Phys. J.* **C75**(10), 476 (2015). doi: 10.1140/epjc/s10052-015-3685-1.
14. CMS Collaboration, Particle-Flow Event Reconstruction in CMS and Performance for Jets, Taus, and MET. (CMS-PAS-PFT-09-001) (Apr, 2009). URL `http://cds.cern.ch/record/1194487`.
15. Y. Gao, A. V. Gritsan, Z. Guo, K. Melnikov, M. Schulze, et al., Spin determination of single-produced resonances at hadron colliders, *Phys.Rev.* **D81**, 075022 (2010). doi: 10.1103/PhysRevD.81.075022.
16. S. Bolognesi, Y. Gao, A. V. Gritsan, K. Melnikov, M. Schulze, et al., On the spin and parity of a single-produced resonance at the LHC, *Phys.Rev.* **D86**, 095031 (2012). doi: 10.1103/PhysRevD.86.095031.
17. I. Anderson, S. Bolognesi, F. Caola, Y. Gao, A. V. Gritsan, et al., Constraining anomalous HVV interactions at proton and lepton colliders, *Phys.Rev.* **D89**(3), 035007 (2014). doi: 10.1103/PhysRevD.89.035007.
18. P. Avery, D. Bourilkov, M. Chen, T. Cheng, A. Drozdetskiy, et al., Precision studies of the Higgs boson decay channel $H \to ZZ \to 4\ell$ with MEKD, *Phys.Rev.* **D87**(5), 055006 (2013). doi: 10.1103/PhysRevD.87.055006.
19. J. Alwall, M. Herquet, F. Maltoni, O. Mattelaer, and T. Stelzer, MadGraph 5 : Going Beyond, *JHEP.* **1106**, 128 (2011). doi: 10.1007/JHEP06(2011)128.
20. A. Belyaev, N. D. Christensen, and A. Pukhov, CalcHEP 3.4 for collider physics within and beyond the Standard Model, *Comput.Phys.Commun.* **184**, 1729–1769 (2013). doi: 10.1016/j.cpc.2013.01.014.
21. J. S. Gainer, K. Kumar, I. Low, and R. Vega-Morales, Improving the sensitivity of Higgs boson searches in the golden channel, *JHEP.* **11**, 027 (2011). doi: 10.1007/JHEP11(2011)027.
22. Y. Chen, N. Tran, and R. Vega-Morales, Scrutinizing the Higgs Signal and Background in the $2e2\mu$ Golden Channel, *JHEP.* **01**, 182 (2013). doi: 10.1007/JHEP01(2013)182.
23. S. Dittmaier, S. Dittmaier, C. Mariotti, G. Passarino, R. Tanaka, et al., Handbook of LHC Higgs Cross Sections: 2. Differential Distributions (2012). doi: 10.5170/CERN-2012-002. URL `http://arxiv.org/abs/1201.3084`.
24. LHC Higgs Cross Section Working Group, Handbook of LHC Higgs Cross Sections: 3. Higgs Properties (2013). doi: 10.5170/CERN-2013-004. URL `http://arxiv.org/abs/1307.1347`.
25. M. Bonvini, F. Caola, S. Forte, K. Melnikov, and G. Ridolfi, Signal-background interference effects for $gg \to H \to W^+W^-$ beyond leading order, *Phys.Rev.* **D88**(3), 034032 (2013). doi: 10.1103/PhysRevD.88.034032.
26. ATLAS Collaboration, Measurement of hard double-parton interactions in $W(\to l\nu)+$ 2 jet events at $\sqrt{s}$=7 TeV with the ATLAS detector, *New J.Phys.* **15**, 033038 (2013). doi: 10.1088/1367-2630/15/3/033038.
27. M. Botje et al., The PDF4LHC Working Group Interim Recommendations (2011).
28. I. W. Stewart and F. J. Tackmann, Theory Uncertainties for Higgs and Other Searches Using Jet Bins, *Phys.Rev.* **D85**, 034011 (2012). doi: 10.1103/PhysRevD.85.034011.

29. CMS Collaboration, Observation of Z decays to four leptons with the CMS detector at the LHC, *JHEP.* **1212**, 034 (2012). doi: 10.1007/JHEP12(2012)034.
30. ATLAS Collaboration, Measurements of Four-Lepton Production at the Z Resonance in pp Collisions at $\sqrt{s}$ =7 and 8 TeV with ATLAS, *Phys.Rev.Lett.* **112**(23), 231806 (2014). doi: 10.1103/PhysRevLett.112.231806.
31. Particle Data Group, Review of Particle Physics, *Chin.Phys.* **C38**, 090001 (2014). doi: 10.1088/1674-1137/38/9/090001.
32. ATLAS Collaboration, Fiducial and differential cross sections of Higgs boson production measured in the four-lepton decay channel in *pp* collisions at $\sqrt{s}$=8 TeV with the ATLAS detector, *Phys.Lett.* **B738**, 234–253 (2014). doi: 10.1016/j.physletb.2014.09.054.
33. CMS Collaboration, Measurement of differential and integrated fiducial cross sections for Higgs boson production in the four-lepton decay channel in pp collisions at $\sqrt{s}$ = 7 and 8 TeV, *JHEP.* **04**, 005 (2016). doi: 10.1007/JHEP04(2016)005.
34. A. Soni and R. M. Xu, Probing CP violation via Higgs decays to four leptons, *Phys. Rev.* **D48**, 5259–5263 (1993). doi: 10.1103/PhysRevD.48.5259.
35. W.-Y. Keung, I. Low, and J. Shu, Landau-Yang Theorem and Decays of a Z' Boson into Two Z Bosons, *Phys. Rev. Lett.* **101**, 091802 (2008). doi: 10.1103/PhysRevLett.101.091802.
36. P. Artoisenet, P. de Aquino, F. Demartin, R. Frederix, S. Frixione, et al., A framework for Higgs characterisation, *JHEP.* **1311**, 043 (2013). doi: 10.1007/JHEP11(2013)043.
37. L. Randall and R. Sundrum, A Large mass hierarchy from a small extra dimension, *Phys. Rev. Lett.* **83**, 3370–3373 (1999). doi: 10.1103/PhysRevLett.83.3370.
38. M. Chen, T. Cheng, J. S. Gainer, A. Korytov, K. T. Matchev, et al., The role of interference in unraveling the ZZ-couplings of the newly discovered boson at the LHC, *Phys.Rev.* **D89**(3), 034002 (2014). doi: 10.1103/PhysRevD.89.034002.
39. Y. Chen, R. Harnik, and R. Vega-Morales, Probing the Higgs Couplings to Photons in $h \to 4\ell$ at the LHC, *Phys.Rev.Lett.* **113**(19), 191801 (2014). doi: 10.1103/PhysRevLett.113.191801.
40. ATLAS Collaboration, Search for new light gauge bosons in Higgs boson decays to four-lepton final states in *pp* collisions at $\sqrt{s}$ = 8 TeV with the ATLAS detector at the LHC, *Phys. Rev.* **D92**(9), 092001 (2015). doi: 10.1103/PhysRevD.92.092001.
41. CMS Collaboration, Search for a Higgs Boson in the Mass Range from 145 to 1000 GeV Decaying to a Pair of W or Z Bosons, *JHEP.* **10**, 144 (2015). doi: 10.1007/JHEP10(2015)144.
42. ATLAS Collaboration, Search for an additional, heavy Higgs boson in the $H \to ZZ$ decay channel at $\sqrt{s}$ = 8 TeV in *pp* collision data with the ATLAS detector, *Eur. Phys. J.* **C76**(1), 45 (2016). doi: 10.1140/epjc/s10052-015-3820-z.